# CRITICAL DYNAMICS IN MICROGRAVITY

# (DYNAMX)

*SCIENCE REQUIREMENTS DOCUMENT*

**(JPL Document Number D-18698)**
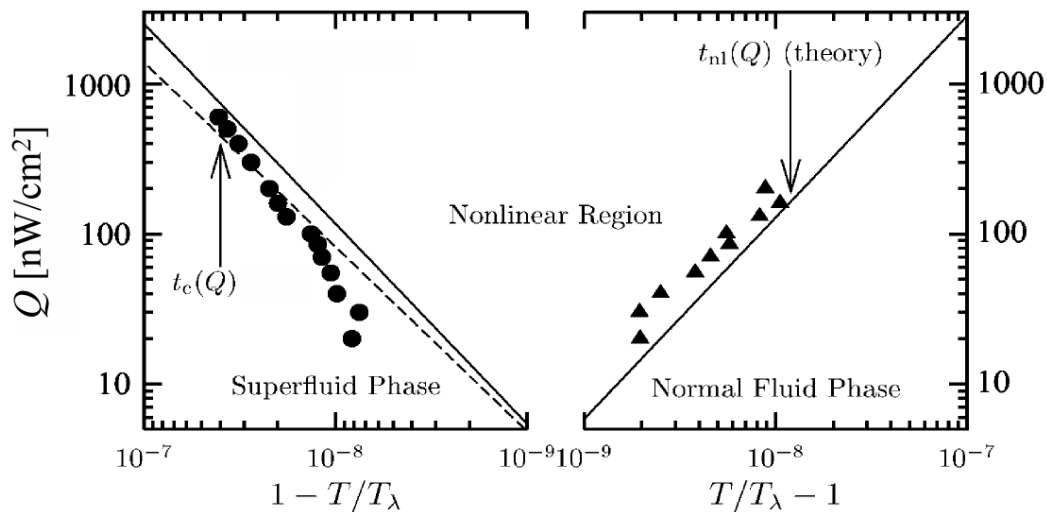


*When driven away from equilibrium by a heat flux Q, the superfluid transition in $^4$He evolves from a simple critical point into a fascinating and complex nonlinear region, where the onset of macroscopic quantum order is masked by Earth's gravity. This is what we know, and how we may learn much more on Earth orbit.*

*31 May, 2000*

*DEPARTMENT OF PHYSICS AND ASTRONOMY*

*UNIVERSITY OF NEW MEXICO*

# Table of Contents

# 6    Flight Experiment Plan

# 7    Prior published work    

# 8    References    

# 9    List of Acronyms    

# 1. Executive Summary

The concept of the continuous phase transition is one of the most important in modern science, having a profound influence on our understanding of fundamental physics, physical chemistry, cooperative phenomena, and complex systems. Many engineered systems and measurement devices exploit the properties of materials near their critical points. The theory of critical phenomena requires an infinite system in equilibrium. In reality, every physical system is to some extent finite, and every system undergoes phase change at some non-zero rate. Hence every physical system violates both conditions mentioned above for a critical phase transition, even in a perfectly pure system. Real systems under study depart from their predicted divergent thermophysical properties at a predictable distance from the critical point, which becomes smaller as the system becomes closer to ideal.

Critical Dynamics in Microgravity (DYNAMX) will use the most pure system available, namely the superfluid transition in pure $^4$He, to explore how out-of-equilibrium conditions modify the nature of continuous phase transitions. No prior flight experiment within the Microgravity Program has investigated dynamical aspects of critical phase change. DYNAMX will provide a fundamental understanding of these new physical phenomena and an experimental test of our most sophisticated, renormalized theories of dynamical effects near a critical point.

Experimentally, a small cylindrical sample of superfluid helium is maintained in microgravity with a heat flux Q entering from one end of the cylinder, and removed from the other, as depicted in figure 1. A small additional heat flux $\Delta Q = 0.01$ Q is provided to the warm endplate to permit the cell to warm up slowly, at about 50 pK/s, until the normal fluid interface forms near the heated endplate. The interface will advance by each of three temperature probes embedded in the cylindrical cell's sidewall at a speed of only 0.1 µ/s. The temperature profile behind the interface is measured as the interface moves past the sidewall probe. Temperature profiles will be obtained at twenty values of Q between 10 - 100 nW/cm$^2$, using three probes of different thickness to remove experimental artifacts.

These thermal profiles will be used to determine the thermal conductivity of the liquid $^4$He as a function of temperature exceptionally close to the superfluid transition. Similar data taken on Earth suggest that gravity fundamentally affects the conductivity by limiting the range over which phase fluctuations of the superfluid order parameter persist. Furthermore, dynamic renormalization group theory predicts that these profiles taken at many different values of Q should all collapse onto the same curve (that is, quasi-scale) when they are transformed in a manner that depends only on temperature and on Q. The quasi-scaling prediction cannot be tested accurately on Earth, since gravity compresses these profiles to a width that cannot be measured with current technology. In microgravity, however, these profiles achieve their big, fundamental width which is easily measured. Finally, DYNAMX will determine if there is a temperature difference between when the interface enters and leaves the experimental cell through the bottom endplate. Data obtained in this manner will be used to determine if the superfluid transition is hysteretic. While the superfluid transition has been predicted to be hysteretic

under a heat flux, such hysteresis has never been observed, despite careful experimental measurements on Earth.  DYNAMX will determine if hysteresis is masked by gravity.

   These measurements will, for the first time, explore the fundamental nature of the non-equilibrium phase transition to superfluidity in $^4$He, unmasked by gravitational effects.   This will provide conclusive experimental tests of the most advanced, renormalized theories of dynamical phase change.   Furthermore, through a close comparison to extensive ground-based measurements, the systematic effect of gravity on the thermal profile, and hence on the extent of quantum fluctuations, will be inferred. These results will have a profound scientific impact in several ways, including our understanding of dynamic critical phenomena, our understanding of quantum liquids and quantum phase fluctuations, and possibly on closely related fields, such as cosmology and quantum statistics.
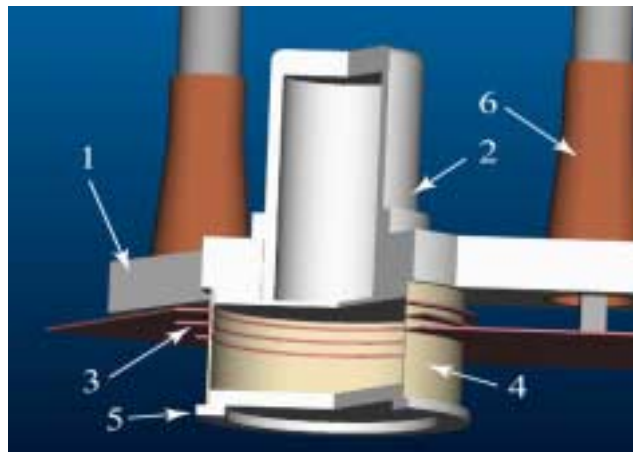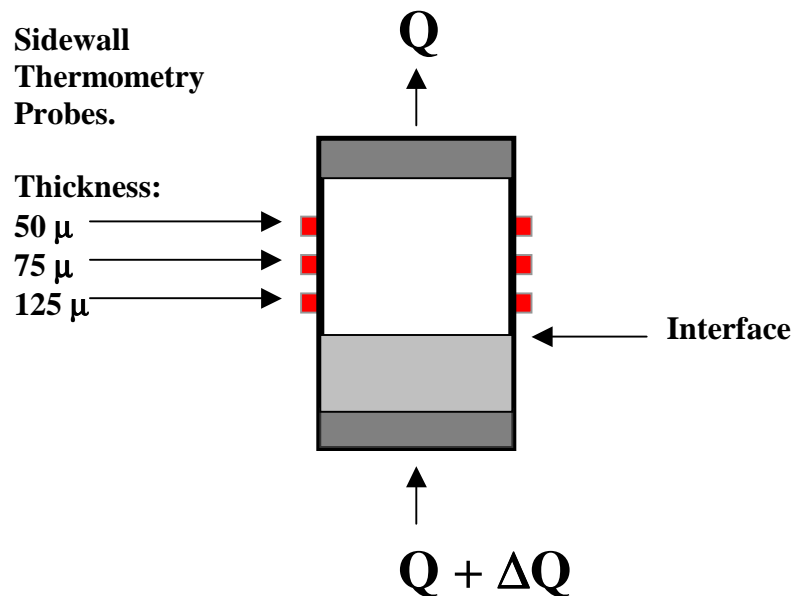


**Figure 1**: Top: A conceptual depiction of the cell showing probes of the three different thickness used on Earth, and which are proposed for the flight experiment.  Bottom: Scale drawing of the cell displayed in a cut-away view, with 1) the cool end-plate, 2) the bubble chamber, 3) the sidewall thermometry probes, 4) the insulating sidewall, 5) the warm end-plate, and 6) the mini high-resolution thermometer mounts.

## 2. Introduction

The superfluid transition in pure $^4$He is an excellent model system of a continuous phase transition, since it may be made absolutely pure chemically [1]. Physical impurities, such as vacancies, dislocations, and grain boundaries that are present in solid-state materials do not exist in superfluid helium. Since $^4$He is uncharged and only very weakly diamagnetic, it is not affected appreciably by stray electromagnetic fields [2].

Critical phenomena studies of static or near-static properties in many different materials have demonstrated relatively good agreement between theory and experiment, demonstrating that critical phenomena theory is likely to be correct in its unobtainable, ideal limit [3-6]. An exceptionally powerful theoretical technique, called the Renormalization Group (RG), has been used to predict the universal properties of real, finite systems near their critical points and dynamical effects near criticality [7]. These finite-size scaling and dynamic effect predictions have been tested experimentally near the lambda transition in $^4$He, confirming the impressive predictive power of the RG technique.

Recently these RG techniques have been extended to predict the behavior of liquid $^4$He driven far from equilibrium near the lambda point [8 - 10]. This is very important, since every critical phase transition in nature has occurred at some finite rate, and hence has occurred intrinsically out-of-equilibrium at some level. Hence these recent RG predictions, and other theories [11, 12], deserve close experimental attention.

DYNAMX has observed dynamic departures from linear response in our heat transport measurements in our ground-based experiments within 20 nanokelvins of the superfluid transition temperature [13]. The measurements described below represent the first conclusive observation of the breakdown of Fourier's Law resulting from the large fluctuations of the order parameter near a critical point. In other measurements, DYNAMX has observed the formation of a self-organized critical state, where the temperature gradient across the liquid helium remains constant and equal to the pressure-induced gradient in the superfluid transition temperature $T_\lambda$ as the heat flux was varied over three orders of magnitude [14]. The self-organized state leaves the entire sample at a uniform distance from criticality. While these self-organized measurements display an apparent uniformity across the sample cell, the helium is actually driven far from equilibrium. In the self-organized critical state the system 'self-adjusts' its temperature, and thus the fluctuations of its order parameter above $T_\lambda$ to obtain the correct thermal conductivity to maintain a constant thermal gradient equal to $\nabla T_\lambda$ as Q is varied [14]. Remarkably, below $T_\lambda$ the system still self-organizes, probably by 'self-adjusting' the rate of phase slips in its macroscopic order parameter [11]. Self-organization, along with the effects of gravity on the correlation length, make the system very complicated, and are the focus of current ground-based research efforts, both experimental and theoretical.

The inhomogeniety in $T_\lambda$ caused by the pressure gradient across the $^4$He sample created by the weight of the helium column is predicted to be larger than the inhomogeniety created by the heat flux in the middle of the nonlinear region for Q < 70 nW/cm$^2$. Hence the primary range for the measurements on Earth-orbit will span the range 10 < Q < 100 nW/cm$^2$, and the extended range of measurements will span 5 < Q < 200 nW/cm$^2$. A full decade of measurements will be made in the nonlinear region, with

adequate data at higher heat flux to make a solid connection with measurements made on Earth in the linear region. These measurements of the nonlinear thermal conductivity will be made at a level of at least 5% accuracy over the temperature range from $T_\lambda$ to $T_{nl}(Q)$, where $T_{nl}(Q)$ is the temperature defined by Haussmann and Dohm (HD) [8] above which linear response is observed to within the experimental accuracy. In addition, the thermal profile near the interface will be recorded and compared to the predicted quasi-scaling function of HD. If such quasi-scaling behavior is observed, then the Q-dependence of the interfacial thickness, and hence the Q-dependence of the correlation length, will be inferred from the data.

While the orbital measurements will provide quantitative data on the thermal conductivity in the nonlinear region and the Q-dependence of the correlation length, other more qualitative aspects of the nature of the superfluid transition driven far from equilibrium will also be observed. Many theorists have predicted that the superfluid transition under a heat flux will be hysteretic, but no hysteresis has yet been detected experimentally in Earth-based measurements [15]. These measurements have been sensitive enough to detect hysteresis at a level of 10% of the theoretical prediction [16]. If the Earth-based null result is due in part to the presence of gravity on the superfluid transition, then the orbital measurements may be the first to detect it. These orbital measurements will be capable of detecting hysteresis as small as 1% of the predicted value. Furthermore, recent results [17] suggest that the temperature above which superfluid counterflow fails suddenly, called $T_c(Q)$, may in fact be associated with a boundary instability rather than a bulk transition. Other theoretical results [10] predict that the isothermal He-II phase, which has been observed on Earth above the interface, may actually develop a temperature gradient in microgravity. These $T_c(Q)$ measurements will be repeated on orbit, and any thermal gradient above 1 nK/cm in the He-II phase will be detected experimentally.

DYNAMX will result in the first highly quantitative measurement of dynamical effects on a nearly continuous phase transition in the limit where linear response fails even qualitatively, since the He-I / He-II interface does not exist in microgravity without a heat flux. Hence the He-I / He-II interface is an intrinsically nonlinear entity in microgravity. These measurements will also provide information on how macroscopic quantum order emerges in a system driven away from equilibrium in a highly controlled manner. Such data, taken free of hydrostatic gradients inevitable on Earth, will prove useful to a wide variety of scientific communities.

The effects of heat, momentum, charge, and mass transport near critical points has been an active field of research for many years in numerous physical systems [18]. While the static properties near the superfluid transition in [4]He have been studied extensively over the last fifty years, relatively little research has been conducted to explore the dynamical properties of the superfluid transition driven far from equilibrium near criticality. Most of the conclusive data with regard to these dynamic properties near the superfluid transition has emerged only recently. Such work is reviewed briefly below.

## 2.1. Superfluid transition in a heat flux

The singular behavior of various transport properties near continuous phase transitions was first predicted on the basis of mode-coupling theory by Ferrell *et al.* in

1967 [19]. This powerful theoretical technique, which became known as dynamical scaling theory, lead to the prediction of the divergence of the thermal conductivity in pure $^4$He as the superfluid is approached from above. The divergence results from fluctuation in the superfluid order parameter that becomes large as the superfluid transition is approached. The predicted divergence in the normal fluid thermal conductivity at $T_\lambda$ was rapidly confirmed experimentally by Ahlers [20] at Bell Labs, and by Kerrisk and Keller [21] at UNM.

Below the superfluid transition, dynamic scaling predicts that the largest wavevector, k, available for heat transport near the superfluid transition scales as the inverse of the correlation length $\xi$, $\xi = \xi_o\, t^{-\nu}$, where $\nu = 0.672$ [22], $\xi_o = 3.4 \times 10^{-8}$ cm, and $t = (T - T_\lambda)/T_\lambda$. The correlation length provides a measure of the range of fluctuations of the gradient of the phase of the superfluid order parameter near a critical phase transition. Notice that the correlation length is of atomic scale far from the superfluid transition, however it becomes large (about 300 microns) as the superfluid transition is approached to within a few nanokelvins. The heat flux $Q_s$ carried by counterflow, in the absence of mass flow is given by $Q_s = -\rho_s S T_\lambda w$ near the superfluid transition. Here $\rho_s$ is the superfluid fraction, S is the entropy, and w is the counterflow velocity near $T_\lambda$ which is given by $hk/2\pi m_4$, where h is Planck's constant, and $m_4$ is the mass of the helium atom. Since $\rho_s$ and k both scale as $1/\xi$, and since $\xi$ scales as $t^\nu$, $Q_s$ scales as $t^{2\nu}$. As the superfluid transition temperature is approached from below, the maximum value of k becomes very small, resulting in a very small maximum value for $Q_s$. If Q exceeds $Q_s$, then the counterflow state fails catastrophically and a thermal gradient suddenly appears across the helium sample, since now the heat must be transported by normal diffusive means. For any given heat flux Q, the temperature $T_c(Q)$ at which the sudden onset of a thermal gradient is observed must therefore decrease with increasing Q, implying that a region of temperature $T_c(Q) < T < T_\lambda$ exists where the helium is resistive, but where the helium would suddenly display heat superconductivity if Q were lowered isothermally. As described below, over this region (in fact over a region twice as wide centered on $T_\lambda$ [8, 13]), the response of the helium to the heat flux is strongly dependent on the heat flux itself. This region is called the nonlinear region.

## 2.2. Theoretical predictions of the nonlinear region

As early as 1969 Mikeska [23] studied the stability of superfluid counterflow using a free energy analysis, and predicted the existence of the nonlinear region. Mikeska argued that the increase in the free energy of the He-II phase by counterflow should decrease the superfluid order parameter, and hence $\rho_s$. These effects were studied systematically by Mikeska in 1969, although Mikeska was only able to roughly estimate $d\rho_s/dw$ using experimental considerations. Later, Ginzburg and Sobyanin [2] developed a field-theoretic treatment of the superfluid order parameter, which they used to refine their theoretical estimate of the variation of $\rho_s$ with w. These dynamical effects on $\rho_s$ were observed deep within the superfluid phase, and hence well away from the critical region, in superfluid oscillator experiments [24] and in measurements of the critical counterflow velocity as a function of the container size [2]. Careful measurements of these nonlinear effects in the critical region, where fluctuation effects are important, were made only recently [13,14,17].

In 1983 Onuki predicted that the width of the nonlinear region would scale as $Q^{-1/2}$, and that the depression of the superfluid transition temperature, $T_\lambda - T_c(Q)$, would scale roughly as $Q^{0.81}$. Onuki later revised his estimate and predicted that $T_\lambda - T_c(Q)$ would be proportional to $Q^{1/2\nu}$. In 1992, Haussmann and Dohm predicted the existence of the nonlinear region based upon a renormalized field theoretic analysis [8,9]. This analysis was based on the 'Model F' Hamiltonian of Halperin, Hohenberg, and Siggia [25], which had been used as the basis for predictions [26] of the linear thermal conductivity near $T_\lambda$. The linear thermal conductivity has been experimentally verified over a wide range of temperature and pressure [5,6]. The nonlinear region predicted by HD is displayed as a function of Q in figure 2, along with data from DYNAMX [13] which experimentally determined the boundaries of the nonlinear region. HD also calculated the thermal conductivity within the nonlinear region for $T > T_\lambda$, but in the absence of Earth's gravity. HD predicted the thermal conductivity in the middle of the nonlinear region, $\kappa(t = 0)$, would scale with $Q^{-0.31}$ and that the temperature span of the nonlinear region, $\delta T_{nl}$, would scale as $Q^{1/2\nu} = Q^{0.74}$. From these predictions the width of the nonlinear region, $W$, should scale as the temperature span of the nonlinear region divided by the temperature gradient in the middle of the nonlinear region. Hence $W$ should scale roughly with $\delta T_{nl} / [Q / \kappa(\epsilon = 0)]$, and thus with $Q^{-0.39}$. A complete analysis [8] showed that the width of the nonlinear region, the Q-dependent correlation length $\xi(Q)$, and the interfacial thickness, all should quasi-scale as $Q^{-0.55}$. Typically the width of the nonlinear region is defined as the interfacial thickness, and is approximately four times the Q-imposed limit of the correlation length.
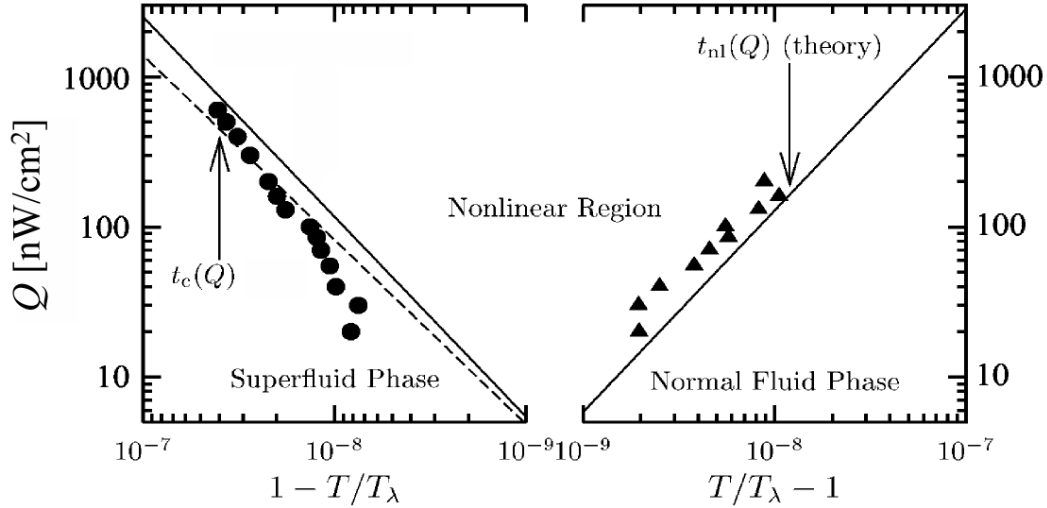


**Figure 2**: The nonlinear region, as predicted by Haussmann and Dohm [8], and experimental data on the extent of the nonlinear region from DYNAMX ([13]).

HD predict [8] that the thermal gradient in the nonlinear region will quasi-scale with Q, as displayed in figure 3. If such a quasi-scaling is confirmed in DYNAMX, then the Q-dependence of the correlation length, and hence the interface thickness, may be inferred from the data. Conceptually, the nonlinear region may be thought of as the distance over which the thermal gradient times the distance is comparable to the temperature difference from criticality $(T - T_\lambda)$ [11]. In the framework of dynamic critical phenomena [19], the nonlinear region is the region over which the spectrum of thermal excitations that form the normal fluid are biased substantially by the transport, so that they no longer have a momentum that averages to zero. This compelling microscopic interpretation of the nonlinear region has been proposed recently by Prof. R. Ferrell.
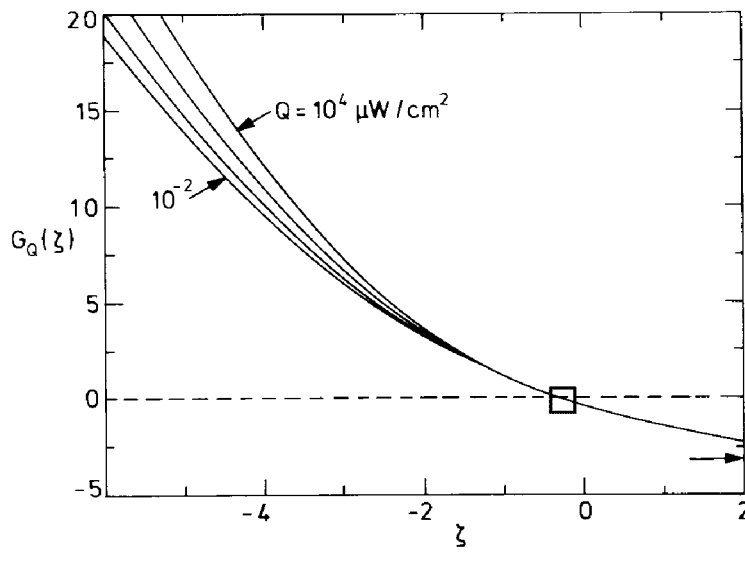


**Figure 3**: The quasi-scaling prediction [8] from HD for the thermal profile in the nonlinear region. Here $G_Q(\zeta)$ is the temperature rise above $T_\lambda$, in units proportional to the depression of the superfluid transition with Q (hence scaled by $Q^{1/2\nu}$), and $\zeta$ is distance, in units proportional to the Q-dependent interfacial thickness (hence scaled by $Q^{-1/2}$). The size of the box on the quasi-scaling curve displays the anticipated experimental uncertainty in our microgravity measurements near the middle of the nonlinear region.

Recent work by Weichman *et al*. [11], and by Haussmann [10], have predicted the nature of the nonlinear heat transport under a constant acceleration due to Earth's gravity. While Haussmann's theory has been developed using RG technique, its validity is limited to the range $Q > 70$ nW/cm$^2$. Unfortunately the region of greatest experimental interest falls at low-Q, where no renormalized theory exists for the heat transport in the nonlinear regime under gravity.

## 2.3. DYNAMX experimental design summary

A simplified view of the experimental cell used in DYNAMX is displayed in figure 1. An all-metal, cylindrical liquid helium cell of 2.3 cm diameter contains three sidewall thermometry probes of different thickness along its 0.9 cm length. A heat flux Q passes

in the bottom and out of the top of the cell. When the cell is entirely in the He-II phase the helium is isothermal, and the probes all read the same temperature. As the cell temperature is increased, an interface to He-I will form at the bottom of the cell and advance toward the top with an interface velocity $v_I$. When the interface arrives at a thermometry probe, that probe suddenly begins to warm much more rapidly than the other probes that are still in contact with the He-II. As the interface advances to a height z above the probe, the probe temperature $T_p$ will measure the corresponding temperature at that position in the normal fluid, provided that the interface advance is slow enough to permit a quasi-static measurement of the thermal gradient. A small but significant correction to the temperature profile $T_p(z)$ is applied to account for the heat that travels up the cell's sidewall and flows back into the helium through the thermometry probe. All of the heat transport properties of the helium of interest to DYNAMX may be obtained from the corrected temperature profile T(z). Only the hysteresis search requires a separate measurement procedure.

The thermal conductivity may be inferred from T(z) simply by dividing the constant heat flux Q by the derivative dT/dz. This derivative may be calculated directly from the temperature profile, or it may calculated by dividing the measured rate of change of the corrected probe temperature, $dT/d\tau$ (here $\tau$ is time), by the interface velocity $v_I = dz/d\tau$. The temperature corresponding to the measurement is just T(z), which is usually recorded as the rise above $T_c(Q)$, where $T_c(Q)$ is the temperature of the probe immediately before it begins to warm rapidly. The reduced temperature corresponding to the measurement is $t(z) = (T(z) - T_\lambda) / T_\lambda$, where $T_\lambda$ is taken to be the value of $T_c(Q)$ in the limit Q→ 0.

An experimental check for hysteresis is obtained by noting the temperature of the He-II with each of the three probes as the interface first enters the cell. The formation of the interface at the warm end of the cell is readily detected by a sudden decrease in the warming rate of all three thermometers as part of the heat flux supplied to the bottom endplate goes into establishing the thermal gradient in the newly formed He-I phase. Once the He-I phase has clearly entered the cell, then the heat extracted from the top end of the cell is increased slightly to reverse the advance of the interface. The temperature at which the interface departs the cell, leaving the cell once again in its He-II phase, is compared to the temperature at which the interface entered. Any difference in these temperatures above the noise level is evidence of hysteresis in the transition. The same procedure may be applied to search for hysteresis at the top endplate, except now the interface will form as a thin He-II layer near the cool endplate, in a predominantly He-I cell.

In the discussions above, the position z of the interface above the probe must be known. On Earth z is readily obtained by measuring the change in the He-II phase temperature, as read by the probe or probes located above the probe in contact with He-I. The interface position z may be inferred on Earth by $z = \alpha^{-1}[T_{II} - T_c(Q)]$, where $T_{II}$ is the temperature of the He-II above the interface. DYNAMX is conducted at saturated vapor pressure, where $\alpha = 1.273$ µK/cm [27]. When the bottom probe is used to make the measurements, the top two probes may both be used to measure the He-II temperature, along with any apparent gradient in the He-II temperature. No such He-II temperature gradients have been measured in the DYNAMX ground measurements, which have been conducted up to a maximum heat flux of 600 nW/cm$^2$.

In microgravity the ground-based method of inferring the interface position from the superfluid temperature change will not work, since the He-II temperature is expected to remain isothermal, or very nearly so, as the He-I phase advances into it. In microgravity we have to depend on the heat required to develop the thermal gradient in the He-I phase to regulate the advance rate of the interface. The interface is expected to remain flat as the He-I phase advances into the He-II phase [11]. An additional heat flux $\Delta Q$, typically $\Delta Q/Q = 0.01$ to $0.02$, is supplied to the bottom (warmer) endplate in figure 1. $\Delta Q$ provides the heat necessary to provide the enthalpy build-up to establish the thermal gradient across the He-I phase. In the limit that the entire He-I phase remains quasi-static as the interface advances, one may think of the He-I temperature profile shifting up by an amount dz in a time $d\tau$ to create an interface advance rate $v_I = dz/d\tau$. The enthalpy required (per unit cross-sectional area) to affect the thermal profile advance is simply $\Delta Q$ $d\tau$, which must equal the enthalpy in the new slice of He-I next to the warm endplate of width dz. The specific heat at constant pressure near the lambda point, $C_p(T)$, has been very accurately measured on the LPE mission [3]. Hence the derivative of the enthalpy per unit area of the layer with z, dH/dz, is simply

$$\mathrm{dH/dz} = \int_{T_\lambda}^{T_w} C_p(T)dT .$$

The interface advance rate in microgravity is $v_I = \Delta Q$ / [dH/dz]. Here $T_w$ is the temperature of the helium next to the warm end plate, which may be accurately calculated by integrating the heat flow equation (Fourier's Law) using a simple power law fit to our observed thermal conductivity $\kappa$ [13] within 10 $\mu$K of $T_\lambda$: $\kappa(T) = 2.308 \times 10^{-5}$ $[(T - T_\lambda)/T_\lambda]^{-0.39}$ W/(cm K). This gives $T_w - T_\lambda = T_\lambda$ $[1.21 \times 10^4$ (cm/W) Q z$]^{1.64}$. Similarly, the width of the nonlinear region may be estimated by calculating the interface travel distance z between $T_\lambda$ and $T_{nl}(Q)$, using the expression setting $T_w = T_{nl}(Q)$, and using data [13] to determine $T_{nl}(Q)$. The estimated width W of the nonlinear region is 2z, which is equal to the interface position above the probe when the probe temperature equals $T_{nl}(Q)$. This estimate gives $W(cm) = 6.9 \times 10^{-6}$ / $[Q(W/cm^2)]^{-0.50}$, in remarkable agreement with theoretical predictions.

Figure 4 shows probe temperatures as a function of time for each of three probes in our flight prototype cell. These profiles were obtained by extracting a heat flux from the top endplate of the cell and supplying a heat flux of $Q + \Delta Q$ to the bottom endplate. The resulting position of the interface was inferred from the change of the He-II temperature, and compared to the expected position based on the interface advance model discussed in the previous paragraph. The agreement was exceptional, with the residual errors less than 1% over our entire range of Q. Residual differences between the temperature profile and the anticipated profile $T_w(z)$ are displayed in figure 5. The excellent experimental agreement demonstrates the level of stray heat control, and the integrity of previously published experimental results [3,13] that are used in this mode. Figure 6 displays the measured interface velocity $v_I$ as a function of position relative to the warm endplate under Earth's gravity, and the difference between measurements of $v_I$ and the expected interface velocity based on the interface advance model. Again, excellent agreement exists between our data and the model. In microgravity, the interface advance rate will

be much faster, especially at low-Q, since ΔQ will not have to supply the heat necessary to warm up the He-II to permit the interface to advance, as it must on Earth. Figure 7 displays the anticipated interface advance rate in microgravity for ΔQ = 0.01Q. Notice in figure 7 that the interface advance rate is a monotonically decreasing function as Q increases, and that this is not true on Earth, as shown in figure 6. The ground-based model for the interface advance, which results in the excellent experimental agreement displayed in figure 5, has been modified for microgravity conditions and then used in Chapter 6 to calculate the time required to perform each of our data scans during the flight experiment.
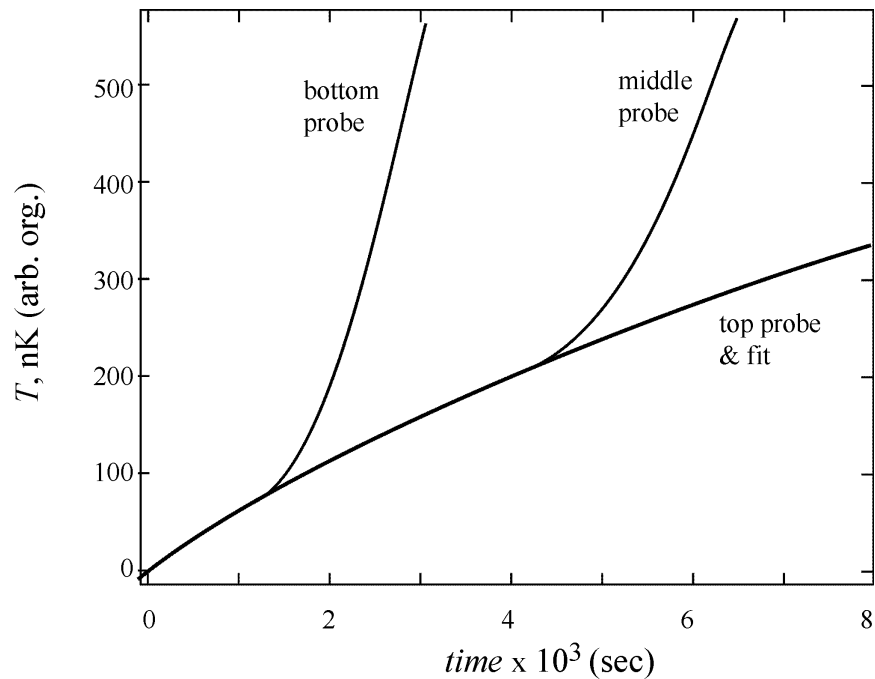


**Figure 4**: Temperature versus time measured at each of the three sidewall probes in the flight prototype cell. The temperature of bottom and middle probes displays a rapid increase as the interface moves by its location. The top probe is always in contact with the He-II phase over this interval of time.
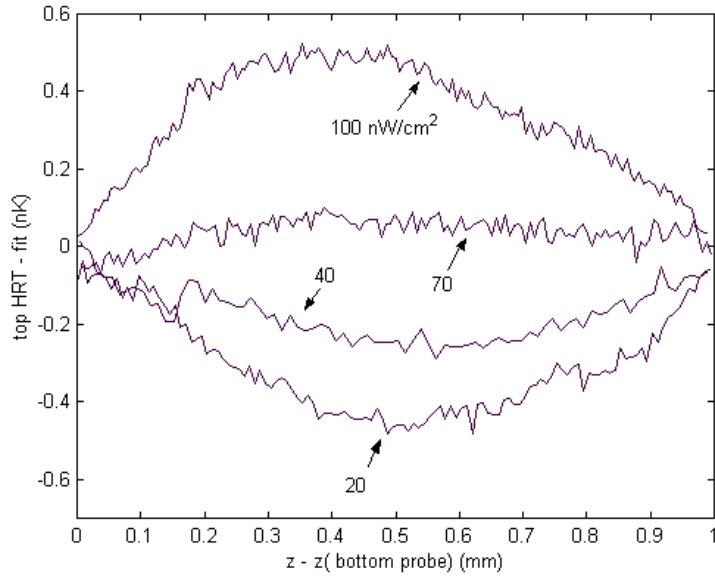
**Figure 5**: The difference between the measured temperature profiles at the bottom probe in figure 4 and the anticipated temperature profile. The anticipated temperature profile is estimated using the interface advance model described in Section 2.3, using independent thermal conductivity [13] and heat capacity [3] measurements.
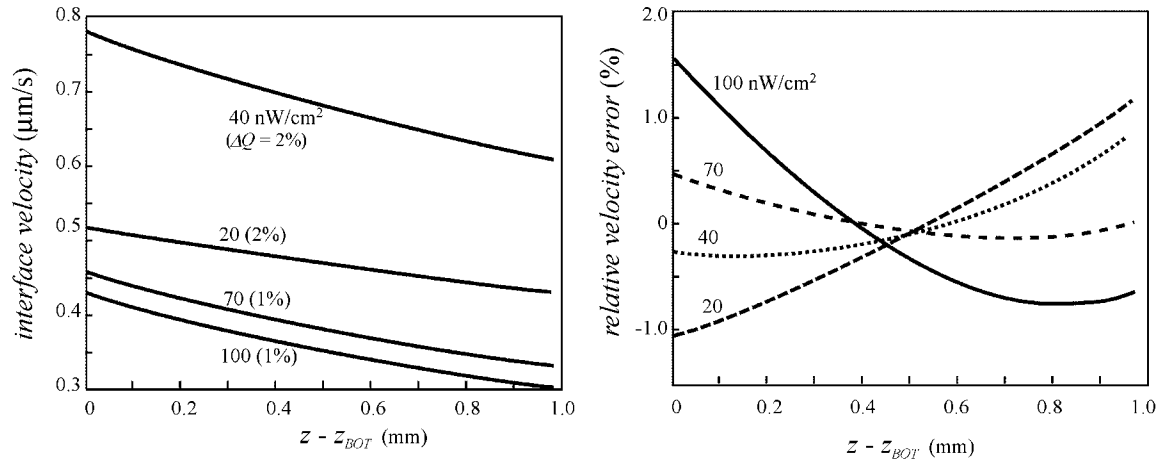


**Figure 6**: The interface velocity $v_I$ measured on Earth and its deviation from the value calculated from the interface advance model.
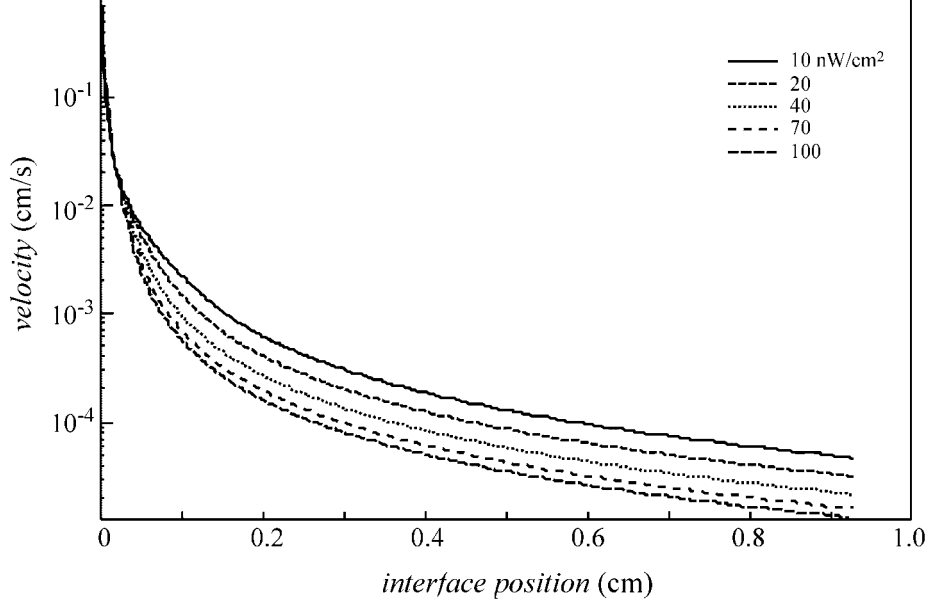
**Figure 7**: The interface velocity in microgravity as a function of interface position within the cell for many values of Q. Here the interface position z is relative to the warm endplate. This plot is inferred from the DYNAMX ground-based data displayed in figures 4 through 7, reconstituted for g = 0.

In the interface advance model we have assumed that the thermal profile in the He-I phase remains quasi-static as the interface advances. The good agreement with ground-based data displayed in figures 4 and 5 support this assumption, however even if the entire He-I layer is not quasi-static, then at least the thin layer of helium behind the interface that we are interested in will be. Even though an additional heat flux $\Delta Q$, equal to 1 - 2 % of Q, is applied to the bottom of the helium layer to affect the interface advance, $\Delta Q$ creates no appreciable error in Q. The variation dQ/dz equals to $v_I C_p Q/\kappa$, so dQ/dz varies with $v_I$, and hence is up to 100 times larger near the warm endplate than it is near the bottom probe. With $\Delta Q = 0.01$ Q, the greatest error in Q at the probe due to the interface advance, which occurs at our lowest value of Q (10 nW/cm$^2$), will be no greater than 0.03% of Q.

For purposes of clarity, we refer to four different temperature ranges in our measurements. First, for $T < T_c(Q)$ we anticipate that the superfluid will be isothermal, or nearly so. Here we will look for the existence of a superfluid thermal gradient, as has been predicted to exist only in microgravity conditions by Haussmann[10]. Second, for $T_c(Q) < T < T_\lambda$, we will measure the thermal conductivity to the limits permitted due to the systematic errors created by the flow of heat out of the sidewall and into the helium. These systematic errors become large when the interface is near the probe, and decrease rapidly as the interface advances well passed the probe. In the range $T_\lambda < T < T_{nl}(Q)$ we will make measurements of the thermal conductivity with an accuracy of 5% in order to conduct a quantitative test of the HD theory[8]. Finally, for $T > T_{nl}(Q)$, we will make adequate measurements to confirm that we have actually achieved the linear region, and

14

to make contact with linear conductivity measurements of other ground-based experimentalists.

In our ground-based work [13], probes of different thickness (25μ, 50μ, 75μ, 100μ, and 125 μ) have been used in a total of four different cells in order to understand the systematic errors associated with the probe. The flight experiment will use the three sidewall probes (50μ, 75μ, 125μ), as displayed in figure 1.

## 2.4. Experiments by other groups

Three distinct ranges of Q are of interest in studies of dynamic effects near the superfluid transition. First, for $Q < 70$ nW/cm$^2$, the hydrostatic variation in $T_\lambda$ across the helium column [27] pushes the system away from criticality more than does the temperature profile that results from Q [13]. In this limit it is desirable to conduct experiments aboard an orbiting laboratory to remove the gradient in the superfluid transition temperature, making the nonlinear region near the superfluid transition much wider and easier to study [28]. Just the opposite situation exists for $Q > 70$ nW/cm$^2$. In the second distinct region, $70$ nW/cm$^2 < Q < 7$ μW/cm$^2$, measurements [29,30] indicate that the bulk superfluid does not develop a measurable thermal gradient before counterflow heat transport fails catastrophically at $T_c(Q)$. Here data on nonlinear heat transport may be taken free from bulk thermal gradients, however the width of the nonlinear region is so small that it is difficult to observe directly. Finally, for $Q > 7$ μW/cm$^2$, a Gorter-Mellink-like [31] bulk thermal gradient becomes substantial compared to our sub-nanokelvin resolution thermometry [32], making the transition to the thermally resistive state less sharp, and hence difficult to study in this high-Q region.

New phenomena have been discovered recently in all of the three ranges of heat flux discussed above. In the highest range of heat flux ($Q > 7$ μW/cm$^2$) a new, dissipative phase of heat transport near the superfluid transition has been observed by Liu and Ahlers [33], and by Murphy and Meyer [34]; however, the interpretation of the nature of the new phase has not yet been determined. For the intermediate range ($70$ nW/cm$^2 < Q < 7$ μW/cm$^2$) the isothermal nature of the helium just below $T_c(Q)$ permits the enhanced heat capacity of the helium under counterflow to be measured. The pioneering measurement has recently been made by Harter *et al*. [17]. Such a dynamic enhancement of the heat capacity just below $T_c(Q)$ had been predicted on the basis of numerous theories [9,12]. In the lowest heat flux region $Q < 70$ nW/cm$^2$, where gravitational effects dominate in nonlinear heat transport, experiments have only been conducted recently [13]. Ground-based DYNAMX experiments have measured these nonlinear effects down to 10 nW/cm$^2$, and disagreement with theoretical predictions [8] at these low values of Q are thought to arise from gravitational effects [10]. Measurements being defined here for the DYMAMX flight experiment on the International Space Station will permit these nonlinear effects to be studied in the absence of gravitational bias. Such measurements will also elucidate the fundamental way that gravitational acceleration influences nonlinear thermal conductivity, through its effect on the correlation length near the superfluid transition. While experiments at these two higher ranges of Q are very important, we do not anticipate that gravity will play an important role. Hence these studies should be continued on the ground, and are not scoped as part of the DYNAMX plan on-orbit.
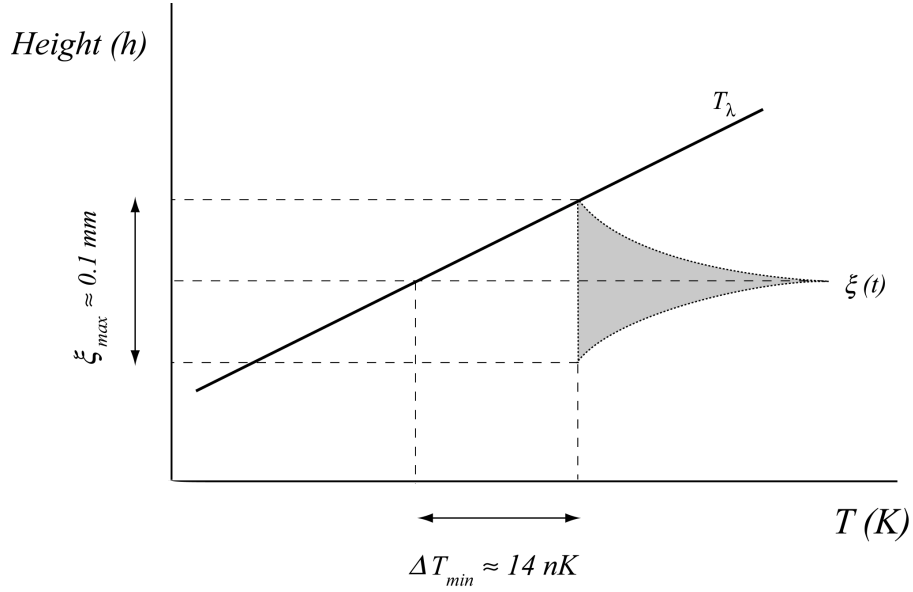
**Figure 8**: Earth's gravity limits the otherwise divergent correlation length to about 0.1mm, resulting in a "closeness of approach" to the critical line of about 14 nK.

## 2.5. Gravitational effects on the heat diffusion and the correlation length

In order to understand how the pressure gradient limits the divergence of the correlation length, consider the situation where the superfluid temperature is approached from above with Q=0 in the infinite system, as sketched in figure 8. Since the superfluid transition temperature varies with pressure, it also varies with height along the helium column as $dT_\lambda/dh = dT_\lambda/dP * dP/dh$. Since $dP/dT_\lambda = -113$ bar/K [35], and $dP/dh = \rho g$, where $\rho$ is the density and $g$ is the gravitational acceleration, then, near saturated vapor pressure, $dT_\lambda/dh = -\alpha = -1.273$ $\mu$K/cm [27]. As the superfluid transition is approached from above, the correlation length increases, resulting in an increasing pressure variation along the correlation length in the direction of gravity. In the ideal static limit the correlation length diverges as $\xi(t) = \xi_o t^{-\nu}$, where $\xi_o = 3.4 \times 10^{-8}$ cm, $t = T/T_\lambda - 1$, and $\nu = 0.672$ [22]. Eventually the point is reached where the isothermal, pressure-induced change in the reduced temperature along the correlation length equals the reduced temperature itself, and the correlation length has reached it maximum value, as shown graphically in figure 8. The maximum value in $\xi$ occurs at a minimum value of the reduced temperature, $t_{min}$, where $\xi(t_{min}) dT_\lambda/dh = T_\lambda t_{min}$. The values listed above give $t_{min} = 3 \times 10^{-9}$, and $\xi(t_{min}) = 110$ $\mu$m. For $t < t_{min}$, gravity will profoundly limit all of the critical singularities by rounding the divergence of the correlation length along the direction of the gravitational acceleration. We anticipate that these gravitational effects on the correlated volume will remain experimentally observable out to reduced temperatures of about $10 t_{min}$, corresponding to 65 nK above $T_\lambda$ on Earth. The

16

gravitational effect on the correlation length discussed above fundamentally changes the nature of the phase transition for t less than about $10t_{min}$.
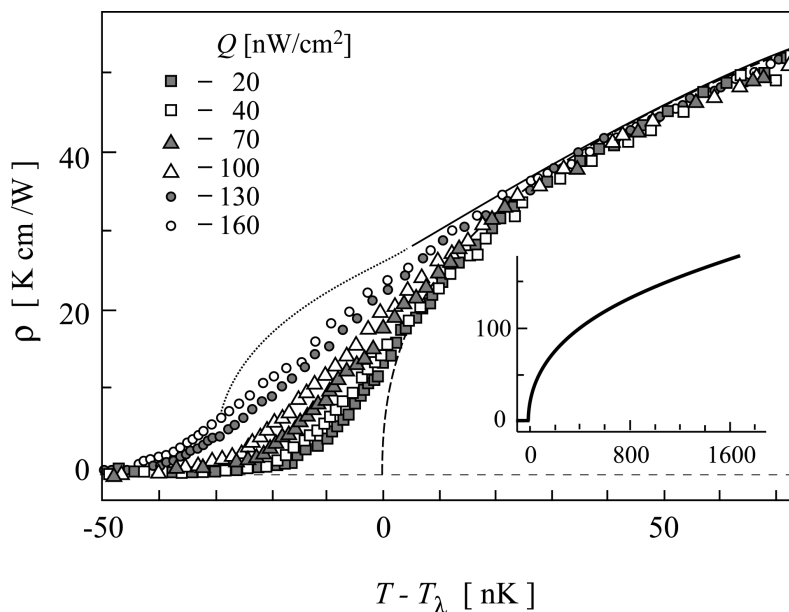


**Figure 9**: Thermal resistivity measurements in the nonlinear region for different values of Q. The long-dashed line is a simple power-law fit to the data in the linear region. The solid line is the prediction of HD at Q = 160 nW/cm$^2$, and the dotted line is a plausible guide for the eye for T < T$_\lambda$, where the HD theory makes no prediction. The insert shows the same data over a wider temperature interval.

In the microgravity environment, the degree to which the divergence of the correlation length (for Q = 0) may be realized experimentally is limited only by the level of experimental control. Hence the critical singularities in the transport properties are anticipated to be uninfluenced by environmental effects to within about 2 nK above the superfluid transition temperature, permitting a factor of thirty times closer approach to the critical point in microgravity than on Earth. The heat flux is predicted to limit the divergence of the correlation length in microgravity [8] to about 110 μm when Q = 60 nW/cm$^2$. Hence the rounding of the static correlation length on Earth is expected to be similar to the rounding of the correlation length in microgravity for Q = 60 nW/cm$^2$. Hence heat transport measurements on Earth should differ dramatically from those made on orbit for Q < 60 nW/cm$^2$. Figure 9 displays DYNAMX measurements of the thermal resistivity of $^4$He very close to the superfluid transition [13]. These data, taken on Earth, show better agreement with the theoretical predictions of HD as Q is increased, since at high-Q gravitational effects are much less important. At lower Q the data show a clear, systematic departure from the HD prediction [8]. Qualitatively, such a trend would be expected due to the gravitational effects discussed above, which have not been considered in the HD theory. A clear understanding of the gravitational effects on the nonlinear region will not be available until our Earth-based data are repeated on-orbit.
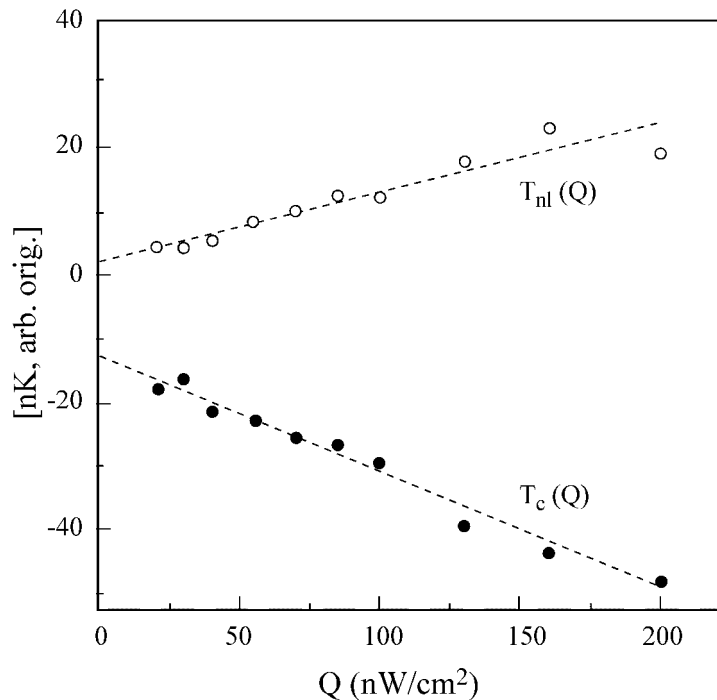
**Figure 10**: DYNAMX ground-based measurements [13] of $T_c(Q)$ and $T_{nl}(Q)$. The fact that these two temperatures do not extrapolate to the same value $T_\lambda$ as $Q$ goes to zero has recently been predicted by Haussmann [10].

In addition to the intrinsic change in the finite-$Q$ thermal resistivity, gravity may also create differences in the depression of the superfluid transition temperature $T_c(Q)$ by a heat flux $Q$, especially in the limit that $Q$ goes to zero. HD predict that both $T_c(Q)$ and $T_{nl}(Q)$ will equal $T_\lambda$ in the limit $Q = 0$ and in the absence of gravity, which is not observed in DYNAMX Earth-based data, as displayed in Figure 10. Recently the difference between $T_c(Q)$ and $T_{nl}(Q)$ in the $Q = 0$ limit has been explained quantitatively by Haussmann [10], who predicts that the difference is purely a gravitational effect that results from the pressure gradient across the interface. According to Haussmann's renormalized theory, the difference $T_{nl}(Q) - T_c(Q)$ should be 19.2 nK, which is only slightly larger than the observed value of 15 nK. Haussmann predicts that the 15 nK gap will go to zero when the measurements shown in figure 10 are repeated in the microgravity environment.

There are well-defined measurements to be made near $T_\lambda$ under a heat flux, as described above, that will test quantitative predictions based on the most advanced, field-theoretic model of continuous phase transitions [25]. Fortunately there are also very interesting qualitative questions to explore which relate to the very nature of the onset of thermal resistance in quantum liquids. Baddar *et al*. measured $T_c(Q)$ using sidewall probes over the same range of $Q$ that was used by Duncan *et al*. who measured $T_c(Q)$ at the cell endplate. The good agreement between these data sets suggests that the isothermal, superfluid state is unaffected by the proximity of a solid wall over the range $0.5 < Q < 10$ $\mu W/cm^2$, suggesting that bulk dynamics dominate boundary effects in this range of heat flux [30]. If true, however, we would expect to see a hysteresis on the order

of the boundary temperature increase created by the singular Kapitza resistance. No such hysteresis has been observed, despite repeated careful measurements by multiple research groups [15, 36]. Recently Chatto [46] has observed that the published rapid heating results [29, 30] which have been interpreted as the bulk superfluid breakdown, may actually be described as an effect associated only with the singular boundary resistance, and not associated with the bulk breakdown at all. Are there fundamental relationships between the boundary and bulk effects that have yet to be postulated? These questions will be explored more accurately on orbit, where the lack of a hydrostatic gradient across the sample will permit us to observe how the superfluid transition occurs in a more ideal, homogeneous pressure condition. In addition, the nature of the superfluid transition in microgravity has been addressed recently by Haussmann [10], and by Weichman *et al.* [11], both using field-theoretic techniques [25]. While their methods are similar, their predictions concerning the dynamics of the phase transition are different. Haussmann, for example, predicts that the He-II phase, which is isothermal on Earth, will develop a measurable thermal gradient in microgravity. Our flight experiment will accurately search for the qualitative features predicted by each of these theories.

In DYNAMX we plan to use values of heat flux in the range $10 < Q < 100$ nW/cm$^2$, where gravitational effects dominate, or are at least comparable to the dynamic effects on Earth. These low values of Q facilitate measurements of the nonlinear region where it is wide compared to our thermometer probe thickness, permitting an exploration of the nonlinear region in more detail. Such exploration includes a search for the predicted [8] quasi-scaling of the interfacial temperature profile. These microgravity experiments, when compared with our ground-based measurements over the same range of Q, will provide a quantitative measurement of the intrinsic, systematic effects of gravity on nonlinear heat transport, which may be extrapolated to higher Q. Thus DYNAMX will quantify the extent of gravitational corrections in other highly precise experiments conducted on Earth.

## 3. Microgravity Justification

The DYNAMX experiment requires the microgravity environment for two reasons, which have been discussed in more detail in Section 2.5. First, DYNAMX intends to unmask the systematic effect of gravitational acceleration on the nonlinear heat transport that has been observed [13] near the superfluid transition. Only by repeating our measurements on orbit will we be able to provide an extensive experimental test of first-principles theory [8, 10, 11, 25] of heat transport in the nonlinear region near the superfluid transition. Furthermore, by comparison of the on-orbit data with Earth-based data we will be able to infer the systematic effects created by Earth's gravity on heat transport near $T_\lambda$, and hence on the correlation length. Second, DYNAMX will realize certain specific measurement advantages that lessen experimental systematic errors and make the experiment easier to do in microgravity.

A detailed discussion of the DYNAMX need for the microgravity environment has been published [37]. In order to test the dynamic RG theory for the breakdown of linear response near the superfluid transition free of gravitational effects [8], and in order to observe the systematic effects of gravity on the correlation length [10] in the nonlinear region, and hence on $T_{nl}(Q = 0) - T_c(Q = 0)$ as described above following figure 10, we must repeat our ground-based measurements [13] in orbit. Such measurements will permit us to understand separately the effects of heat flux and gravity on the diverging quantum correlation length near an apparently continuous phase transition. A precise comparison of microgravity-based data and ground-based data is necessary to observe these effects.

The only valid renormalized theory (which is expected to properly account for the effects of critical fluctuations) of these nonlinear effects assumes no gravitational acceleration [8], so the theory may only be tested quantitatively in the microgravity environment. Extensive measurements have been made of the nonlinear thermal conductivity on Earth, and these data depart from the theoretical predictions in a way that is expected due to gravitational effects, as summarized in Section 2.2.4. Furthermore, the many interesting qualitative theoretical predictions, such as different hysteresis mechanisms [11,16] and a small temperature gradient in He-II [10], have been made for the nature of the superfluid transition in microgravity. None of these qualitative features have been observed on Earth, and these theories are only valid, and hence may only be tested, in microgravity.

In addition to the intrinsic effects of gravity on nonlinear heat transport discussed above, and in a recent publication [38], there are pragmatic measurement advantages associated with the microgravity laboratory. In microgravity the spatial extent of the nonlinear heat transport region expands, making it easier to resolve the thermal gradient within the nonlinear region [15]. Also, at low Q (Q < 70 nW/cm$^2$), the thermal gradient on the normal fluid side of the interface is much smaller than it would be on Earth, making sidewall stray heat corrections smaller by approximately a factor of three, as will be discussed below in Chapter 4. Microgravity reduces the systematic error associated with the sidewall heat conduction near the thermometry probe [39] by about the same factor, as discussed in Chapter 5.

## 4. Flight Experiment Configuration and Control

### 4.1. Introduction

The design of the hardware for the prototype flight Instrument Sensor Package (ISP) assembly is displayed in figure 11. It consists of two coaxial radiation and residual gas shields surrounding an experimental cell assembly. The cell assembly, which includes the cell, thermometers, heaters, and a bubble chamber to maintain saturated vapor pressure (SVP) conditions, has been built using the minimum possible mass (30 g) to avoid systematic errors associated with variations in charged particle heating. The miniature high-resolution thermometers (mini-HRTs) are constructed using a thermometric element constructed of $Pd_{1-x}Mn_x$, where x, the atomic concentration of Mn, is 0.7% to achieve a Curie temperature of 2.1 K, as described in our recent publication [32]. The cell fill line is closed using a cryogenic valve located on the lid of the inner shield, and superfluidity in the helium located in the fill line between the valve and the cell is suppressed using an aerogel thermal break. Nominal values of the thermal resistivity between the stages of the ISP are displayed in figure 12.

### 4.2. Mass considerations

The mass of each of three mini-HRTs is 2.7 g, and the mass of the entire cell assembly, including thermometers, cell, and bubble chamber, is less than 30 g. The total mass must be minimized in order to minimize variations in the charged particle heating of the cell assembly. The cell is cooled by a separate cooling stage controlled using a fourth high-resolution thermometer. The cooling stage and the shield temperatures are controlled by servos, so changes in the charge particle heating levels at these stages may be well compensated by the servo heater. Hence the mass considerations are only critical on the cell assembly, and not on the cooling stage or radiation shields.

### 4.3. Experimental control

On Earth it is possible to infer the change in position of the interface from the change in the temperature of the superfluid phase, due to the pressure dependence in $T_\lambda$ [27]. On orbit, however, we must control the interface advance rate by carefully controlling the excess heat supplied to the warm end over that extracted from the cool end of the cell. The rate of excess heat supply will set the rate of enthalpy build-up in the normal fluid behind the interface, and hence the rate at which the interface advances. A 0.5 cm layer of normal fluid must exist behind the interface in order to control its advance at a sufficiently slow rate past the sidewall probe, as shown in figure 7. A 0.5 cm spacing will assure that the helium remains within 1% of its static condition over our regular measurement range ($T_\lambda$ + 250 nK), as discussed in a separate paper [28]. The normal fluid region also acts as an effective filter against stray heat variations to the cell. Stray

heat into the cell will create a much smaller variation on the interface advance rate as the normal fluid layer becomes thicker.
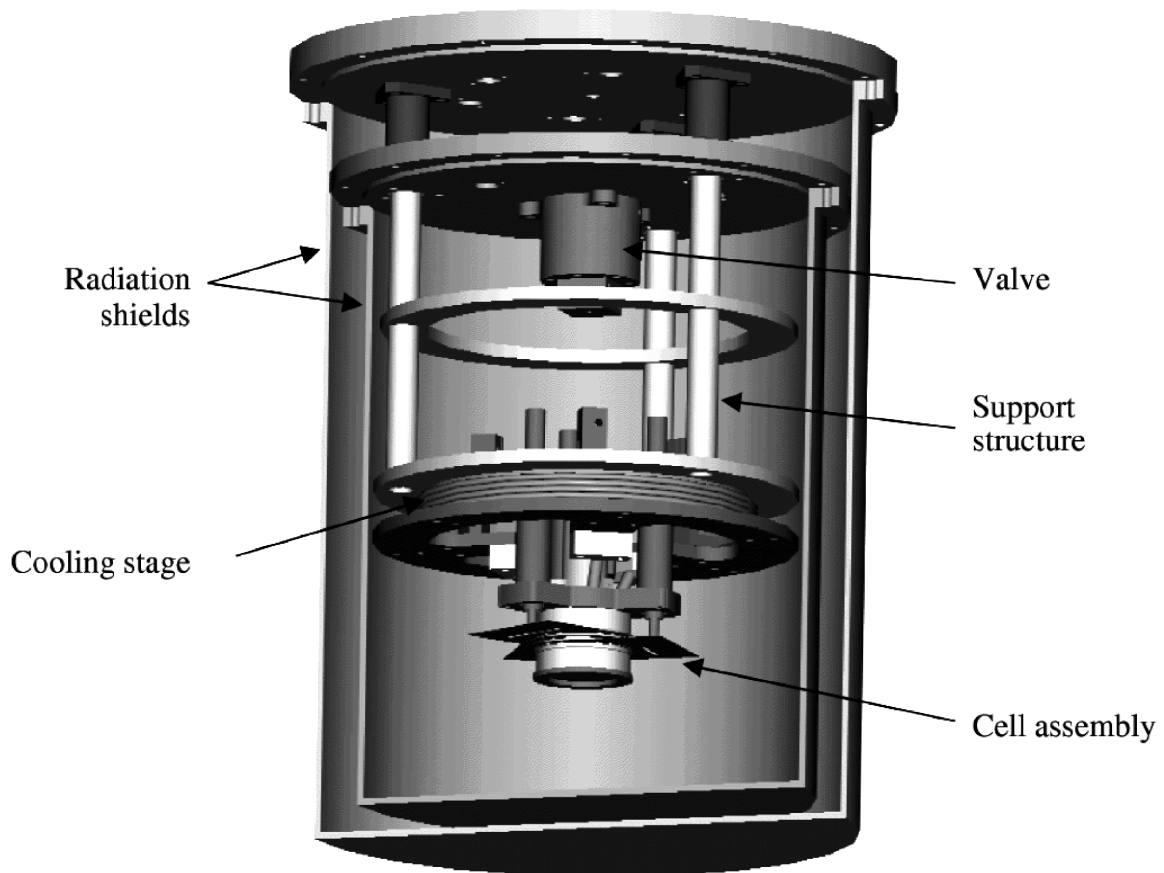


**Figure 11**: Design of the flight prototype Instrument Sensor Package (ISP). This flight prototype hardware has successfully endured shake testing to 7.7 g, exceeding launch-load requirements.

outer shield — 3000 — Iso Stage — 3000 — cooling stage

inner shield — 3000 — cooling stage — 2000 — cell cold end

1e7, 1e7, 1e7 (inner shield to cell cold end)
10, 10, 10 (cell cold end)
5e6, 1.3e5, 5e6, 1.3e5, 5e6, 1.3e5

HRT1 — 40 — helium
HRT2 — 40 — helium
HRT3 — 40

cell cold end — 0.25 — helium — 0.25 — cell warm end

2e5 (to cell warm end)
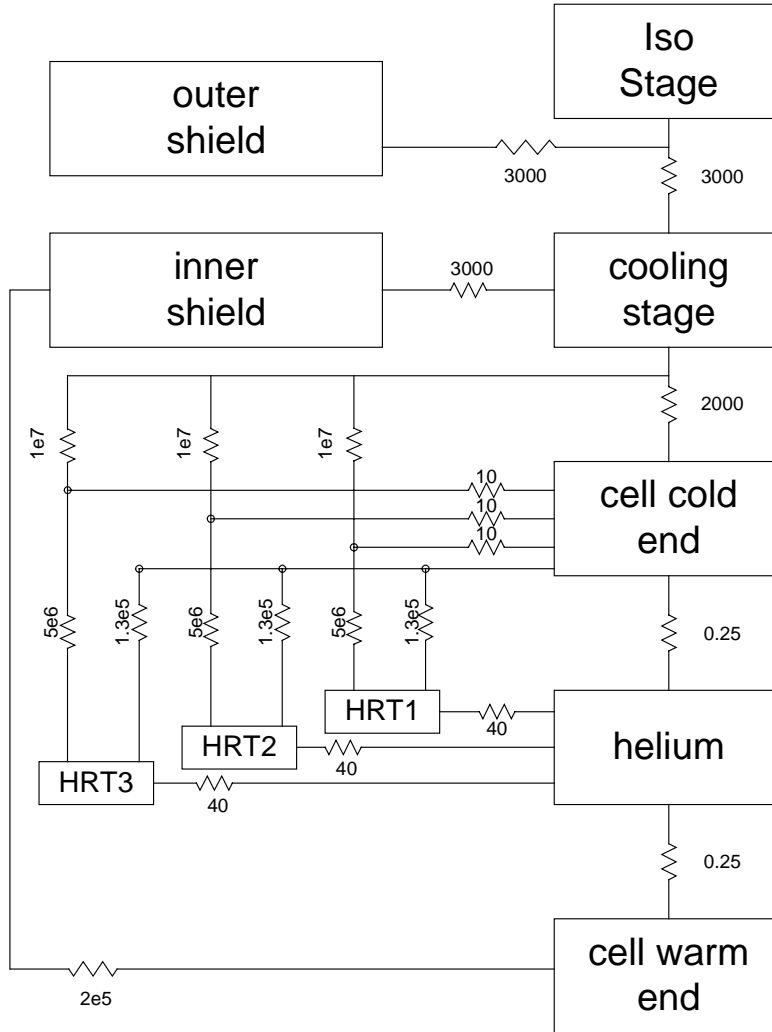
**Figure 12**: Nominal values of the thermal resistivity in K/W between stages in the ISP with the helium in its He-II phase.

## 4.4. Experimental cell

The cell design is displayed in figure 13. It consists of a 75 micron thick stainless steel sidewall that is brazed to 75 micron thick copper probes that extend around the full circumference. The temperature of each of three sidewall probes is measured using a mini-HRT of a new design and a new thermometric element [32]. The flux tubes of these magnetic susceptibility thermometers are charged with a magnetic field between 50-200 gauss using a superconducting magnet. The magnet is located in the liquid helium surrounding the vacuum can during the ground-based measurements, and will be located on the outer radiation shield in the flight experiment. The magnet is used only to charge the mini-HRT's flux tubes during cool-down, and is not energized during the measurements. The entire mass of each sidewall thermometer is only 2.7 grams,

including flux tube. The strict mass requirement on these thermometers assures that the variation in the charged particle heating, which must cool through the thermometry stage, does not create a substantial error in the thermal profile measurements during the data scans.

The thermal profile behind the interface is measured under quasi-static conditions as the interface advances through the cell. The interface position z, relative to the position of the thermometry probe, is inferred from Q and ΔQ, as discussed above in Section 2.3. Furthermore, the time required for the interface to pass two adjacent thermometry probes separated by 1.00 mm will be used as a self-consistent check of the interface advance rate. The interface advance rate measurement provides a real-time check of the level of experimental control. The thermal conductivity data, quasi-scaled temperature profiles, and hysteresis data are inferred from the data as described in Section 2.2.2.
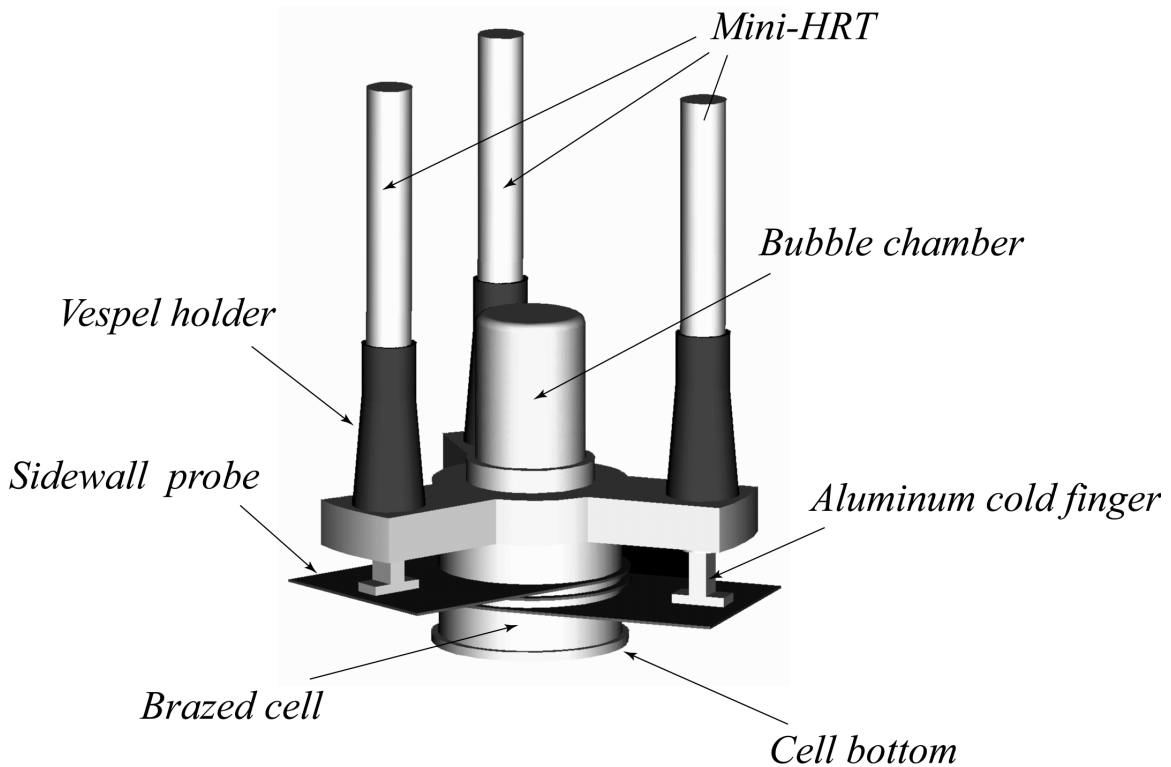


**Figure 13**: The experimental cell. The three sidewall probes are spaced 1.00 mm apart.
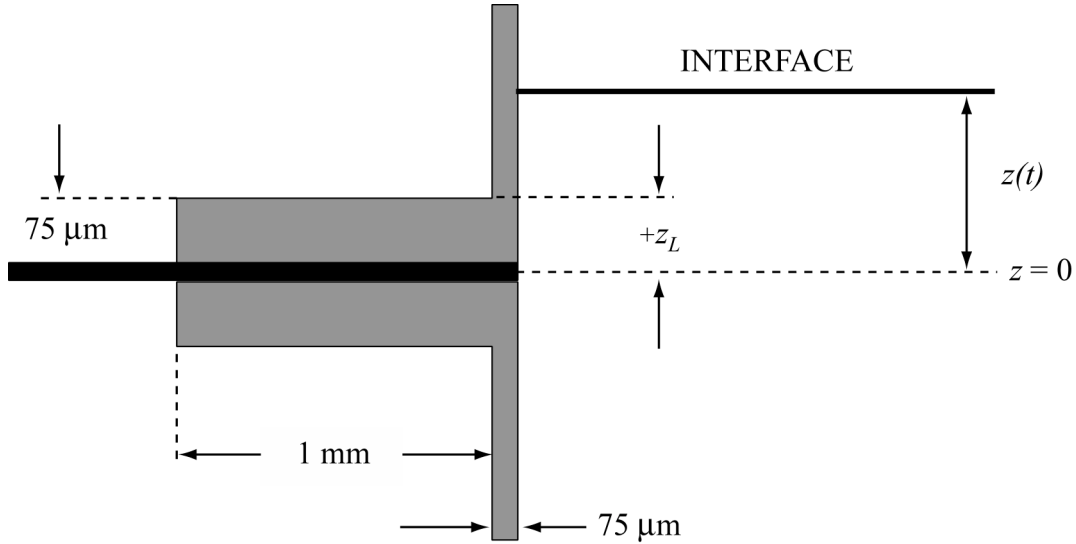
**Figure 14**: The sidewall thermometry probe construction. The interface is above the probe at a height z.

The configuration of the 75 μ thick sidewall probe stage is shown in figure 14. The center of the interface is at a height z above the center of the probe, as shown. As the interface moves by the probe, some of the heat that is transported in the sidewall flows back into the helium along the probe, creating a systematic offset that must be corrected in the data. The sidewall stray heat gives rise to an apparent 'early arrival' of the interface when the helium is in its He-II phase, as shown in DYNAMX ground-based data in figure 15 [13]. Fortunately, the early arrival signature permits the thermometer offset in the He-I phase (when the interface is above the probe) to be accurately estimated. We have used probes of five different thickness (25, 50, 75, 100, and 125 μm), in various combinations, in four different experimental cells during our ground-based measurements.

## 4.5. Data acquisition and analysis

An uncertainty in the correction for the sidewall stray heat exists due to the change in the thermal resistance between the helium and the thermometer as the interface passes the probe and advances to a height z, where data are taken by the probe in the He-I region. The 'early arrival' signature is used to determine the size of the probe correction while the probe is in contact with the He-II phase. In the He-II phase the helium is isothermal, so the early arrival rise shown in the fit region of figure 15 allows us to calibrate the size of the sidewall stray heat, that we must correct later in the He-I phase. Once the sidewall correction is determined, then the estimated error in the thermal conductivity may be determined by taking the ratio of the slope of the correction function to the slope of the corrected data, at each interface position z. The slope of the correction is proportional to the systematic error in the resistivity that results from the sidewall stray heat. The procedure described above has been used to estimate the systematic error in the thermal conductivity, assuming that no probe correction was applied. Clearly the error becomes

very large when the interface is near the probe, corresponding to a measurement temperature near $T_c(Q)$. Our region of greatest measurement accuracy, however, is from $T_\lambda$ to $T_{nl}(Q)$, corresponding to the configuration where the interface is well above the probe's position. We have measured the sidewall error at many values of Q over our experimental range, and find that our 5% measurement objective from $T_\lambda$ to $T_{nl}(Q)$ may not be met over our entire range of Q without first applying a systematic correction for the probe sidewall stray heat. The sidewall heat error correction must be known to an accuracy of 30% in order to achieve our measurement objectives outlined in Chapter 5.
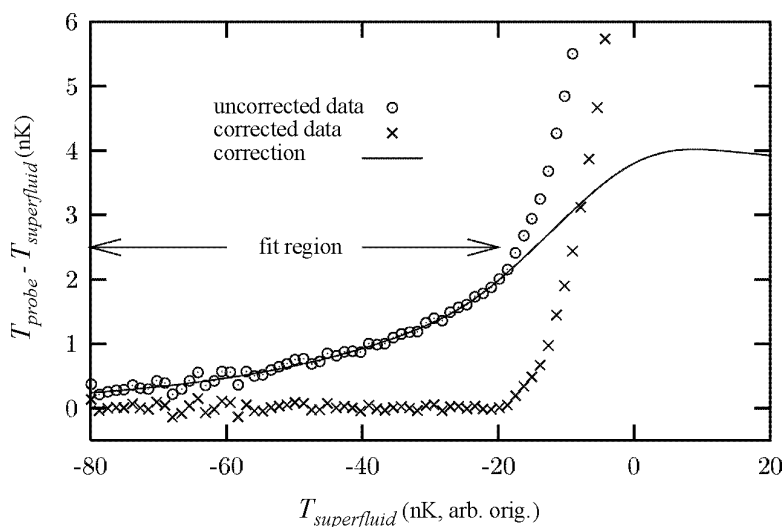


**Figure 15**: The 'early arrival' effect observed in DYNAMX ground-based data [13] at 85 nW/cm$^2$ using a composite material sidewall. The solid line displays the sidewall correction resulting from radial heat flow along the thermometry probe. Notice that it is only the slope of the correction that affects measurement of the thermal resistivity.

The total resistance between the thermometer and the helium is equal to R, where R times the heat flux through the probe gives the temperature difference between the thermometer and the helium in the middle of the cell at the height of the thermometer's stage. Here $R = R_{foil} + R_K + R_{He}$. Here $R_{foil}$, the resistance of the thermometer probe foil, is small (no greater than 0.05 cm$^2$K/W) and constant, since it has no singular temperature dependence. $R_{He}$ is the resistance in the helium liquid, which is approximately equal to $d/(2\kappa_{He})$, where d is the thickness of the thermometer probe foil, and $\kappa_{He}$ is the bulk conductivity of the helium. $R_{He}$ varies from zero in the He-II ('early arrival') region, to 0.11 cm$^2$K/W at the end of the nonlinear region [at $T_{nl}(Q=100$ nW/cm$^2$), which is 24 nK above $T_\lambda$]. Finally, the largest resistance by far is the Kapitza resistance between the helium and the copper probe foil, $R_K$, which we have measured at 2.1 cm$^2$K/W. Here $R_K$ is the sum of a part that is a regular function of temperature through $T_\lambda$, and another part, $R_{Ks}$, which exhibits a weak singularity on each side of the transition. Only $R_{Ks}$ changes from just below $T_c(Q)$ (the end of the fit region shown in figure 15) to $T_{nl}(Q)$. The change in $R_{Ks}$ will create an error in our sidewall heat correction. Measurements of $R_{Ks}$

below $T_\lambda$ [44], and above by Li and Lipa [45], show that $R_K$ varies by at most 3%, which is 0.06 $cm^2 K/W$, from below to above $T_\lambda$ at Q = 100 $nW/cm^2$. Hence the maximum systematic error in our sidewall stray heat corrections from the fit region to the warm end of the nonlinear region will be only about 0.17 $cm^2 K/W$, which is less than 8% of R. Hence we expect that the sidewall stray heat correction can be made to within 10%, which is much better than the required 30% in order to meet the measurement objective of a 5% measurement over the range $T_\lambda < T < T_{nl}(Q)$.

The sidewall stray heat correction, based on experimental data, has been calculated numerically by two independent codes that solve the steady-state heat flow problem in the probe region. Both codes agree, and the corrections are consistent with the interpretation given above.

Sidewall probes of different thickness are used on every cell in order to assure that residual systematic errors associated with the sidewall are not confused with the science data. Our ground-based measurements have used three probes, as displayed in figure 13. The top probe was always in contact with the isothermal He-II, while the interface sweeps past the lower two probes. In figure 16, the resistivity measurements obtained using the upper, 25µ thick, probe are designated $\rho_u$, while those measurements made with the lower, 75µ thick, probe are designated $\rho_l$. Almost all of the thermal resistance between the probe and the helium is due to the Kapitza resistance, so the early arrival effects displayed in figure 15 are smaller in measurements made with the lower probe due to the lower probe's greater surface area against the helium. The measurements in figure 16 demonstrate that any uncorrected systematic error due to the probe's thickness is small compared to the difference observed between the prediction, and the Earth-based data, demonstrating the advantage of using different probe thicknesses in the cell.

As mentioned previously, the ratio of the gradient of the sidewall correction, displayed in figure 15, to the actual temperature gradient provides a measure of the systematic error created by the sidewall probe. Figure 17 displays this ratio as a function of the temperature from our ground-based measurements for Q = 70 $nW/cm^2$. Notice that the systematic error becomes quite large for T near $T_c(Q)$, since there the interface is in direct contact with the measurement probe and hence the sidewall stray heat effect is very large. As the interface advances to higher values of z, and hence the probe warms to a higher measurement temperature, the sidewall correction becomes much smaller. Figure 17 shows that the sidewall probe creates less than a 5% systematic error in uncorrected data for $T > T_\lambda$ at this heat flux, using an earlier cell construction with a Vespel wall [13]. We will correct for the systematic sidewall stray heat effect, reducing the systematic error above $T_\lambda$ to less than 2% over our primary measurement range of Q, provided that the sidewall stray heat correction is accurate to within 30%. Figure 17 provides an estimate of the systematic error that would occur in our measurement range between $T_\lambda$ and $T_{nl}(Q)$ if no sidewall correction were applied. In practice the sidewall stray heat error will be reduced by at least a factor of three by applying the sidewall correction, and possibly further by comparing data taken at each of the thermometry probes of different thickness and refining the sidewall model to correct for any systematic differences above the noise.
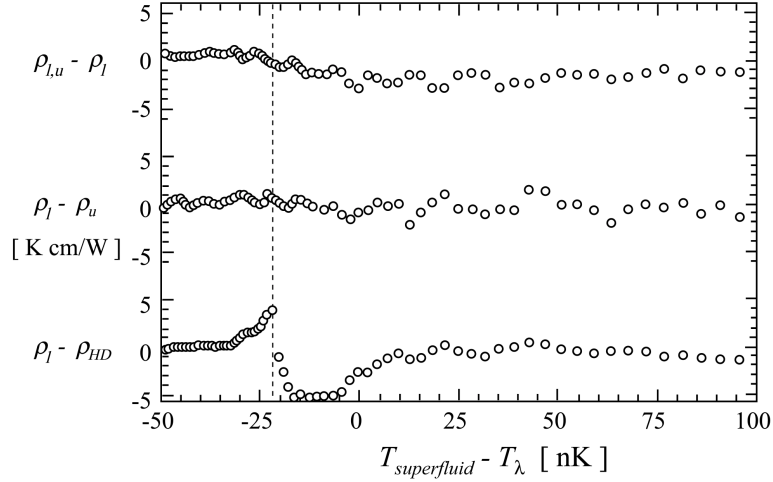
**Figure 16**: A comparison of the DYNAMX resistivity measurements at the lower probe (75 μ) and the upper probe (25 μ). The top data show the difference between resistivity measurements obtained using the uncorrected lower probe data $\rho_{l,u}$ and the corrected lower probe data $\rho_l$. The data in the middle show the difference between resistivity measurements obtained using the corrected upper and lower probes. The bottom data show the difference between the corrected resistivity measurements taken with the lower probe and the predicted resistivity $\rho_{HD}$ [8] for $T_{superfluid} - T_\lambda > 0$. For $T_{superfluid} - T_\lambda < 0$, where HD make no prediction, a simple estimate [33] such as displayed in figure 9 was used in lieu of $\rho_{HD}$. These data were taken with Q=100 nW/cm$^2$, and the dashed vertical line is $T_c$ (Q=100 nW/cm$^2$).
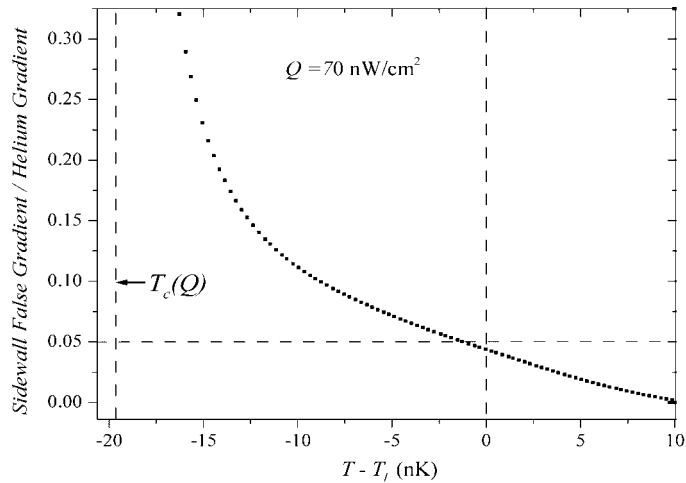


**Figure 17**: The sidewall probe error ('false gradient') as a function of the measurement temperature for Q = 70 nW/cm$^2$, which falls off rapidly as the interface advances above the probe. The sidewall induced error will be removed with an accuracy of 30%. The horizontal line intersects the curve where the uncorrected sidewall probe heat would create a 5% systematic error. The vertical dashed lines are at $T = T_c$(Q = 70nW/cm$^2$), and at $T = T_\lambda$.

## 5. Science Objectives and Requirements

The science objectives, measurement objectives, and the science requirements are discussed here. We also discuss the preliminary functional requirements that have been determined during the development of the DYNAMX flight prototype hardware.

### Science Objectives

The Science Objectives for DYNAMX are numbered SO1 to SO4. They are summarized here:

**SO1**: measure the nonlinear thermal conductivity $\kappa(t,Q)$ near and above $T_c(Q)$, and compare to theoretical predictions.

**SO2**: measure the temperature profile very close to $T_c(Q)$, and from its predicted quasi-scaling with Q, infer the interfacial thickness as a function of Q.

**SO3**: measure variation of the onset temperature $T_c(Q)$ with Q and compare to theoretical predictions.

**SO4**: search for Q-dependent hysteresis near the superfluid transition and compare with theory.

### Measurement Objectives

In order to meet these Science Objectives, a corresponding set of Measurement Objectives have been developed, and numbered MO1 to MO4. Unlike the Science Objectives that remain fixed, these Measurement Objectives have evolved with the DYNAMX technology development assessed through ground-based testing. These Measurement Objectives are:

For $10 \leq Q \leq 100 \text{ nW/cm}^2$, and for $T_c(Q) - 250 \text{ nK} \leq T \leq T_c(Q) + 250 \text{ nK}$ :

**MO1**: measure $\kappa(t,Q)$ to 5% accuracy for $T_\lambda \leq T \leq T_{nl}(Q)$, and to the best extent possible for $T_c(Q) \leq T < T_\lambda$. Here $T_{nl}(Q)$ is the temperature at which non-linearity creates a 5% change in $\kappa$ from its value in the low-Q (linear) limit, as defined by HD [8].

**MO2**: determine the temperature profile for $T_c(Q) \pm 250 \text{ nK}$ to 1.0 nK stability over the course of the measurement scan.

**MO3**: determine $T_c(Q)$ to within 2.2 nK over the full range of Q.

**MO4**: search for hysteresis in the superfluid transition with at least 1 nK resolution.

Given these measurement objectives, together with our understanding of the experimental apparatus, environment, and the helium thermal physics obtained from direct measurement, the science requirements have been derived. Our ability to meet these science requirements has been evaluated against data from ground experiments.

In DYNAMX a stable heat flux is established through the cell, and the resulting temperature as a function of time at each of the sidewall probes is recorded. Hence all of the science requirements center on one, or a combination of: 1) the measurement of temperature, 2) the control of heat applied to the cell or extracted from it, 3) the stability of the sample pressure, and 4) the accuracy of the timing. These four primary requirements are discussed below. In the requirements all stability levels are based on a 10-minute scan duration. Given the width of the nonlinear region and the values of $v_I$ from Chapter 2, all of the nonlinear measurements may be performed within 10 minutes

over the primary range of Q.  Scans of longer duration will be used, however, when the environmental factors permit.  This is discussed in detail in Chapter 6.

## Table 1: SUMMARY OF DYNAMX SCIENCE REQUIREMENTS

Table I provides a summary of the science requirements. Refer to the text for a detailed discussion of each item.

| ITEM | GOAL | REQ | STATUS |
|---|---|---|---|
| **High Resolution Temperature Sensors** | | | |
| Noise in 1 Hz bandwidth (nK, rms. ) | < 0.25 | < 0.3 | 0.10 |
| Thermal time constant (sec.) | < 0.3 | < 1.0 | 0.020 |
| Total mass (g) | 3 | 4 | 2.7 |
| Drift of thermometer ( pK/ sec.) | < 0.02 | < 0.10 | 0.0029 |
| **Sample And Cell Configuration** | | | |
| Probe thickness range ($\mu$m) | 25 - 125 | 50 - 125 | 25 - 125 |
| Probe thickness meas. accuracy (%) | 5 | 10 | 3 |
| Probe spacing (mm) | 1.00 | 0.90 – 1.10 | 1.00 |
| Probe spacing meas. accuracy ($\mu$m) | < 5 | < 10 | < 5 |
| Number of sidewall probes | 3 | 2 | 3 |
| Probe location from cold end (mm) | 2 | 2 | 2 |
| Probe location from hot end (mm) | 5 | 5 | 5 |
| Cell internal diameter (cm) | 2.50 | 2.00 - 2.60 | 2.35 |
| $^3$He content (ppb) | < 1 | < 10 | 0.8 |
| **Heat Flux Control** | | | |
| Range of applied heat flux (nW/cm$^2$) | 5 - 200 | 10 - 100 | 1 - 600 |
| Enthalpy build-up power $\Delta Q$ (% of Q) | 1 | 0.5 - 2.5 | 1 |
| Probe parasitic heat to helium (nW/cm$^2$) | < 2 | < 10 | 0.3 |
| Heat flux uniformity to/from probes (%) | 1 | < 5 | < 5 |
| Measurement accuracy of heat applied to endplates (%) | < 0.2 | < 1 | 0.5 |
| Stability of heat flux applied to the cell (% of $\Delta Q$ per 10 minutes.) | < 1 | < 2.5 | 1 |
| Temperature range for measurements (nK) | $-250 \leq T\text{-}T_\lambda \leq 500$ | $-250 \leq T\text{-}T_\lambda \leq 250$ | OK |
| Time stamp accuracy (ms) | 10 | 100 | LTMPF OK |
| $T - T_\lambda$ measurement accuracy (nK) | 1 | 2.2 | 1 |
| **Acceleration Environment** | | | |
| Total root-mean-square acceleration ($\mu$g$_{rms}$) | < 500 | < 800 | <800 (est.) |
| **Charged-Particle (C-P) Environment** | | | |
| C-P heating variation over datascan (fW/g) | < 165 x (Q/10 nW/cm$^2$) | < 330 x (Q/10 nW/cm$^2$) | OK (est.)[*] |
| Maximum C-P heating rate for measurements (pW/g) | 2 | 2 | OK (est.)[*] |

[*]If the first C-P requirement above is exceeded, then data will not be taken at that Q until the C-P heating stability is back within the requirement.  If the second C-P requirement is exceeded, then helium physics data in the preliminary range of Q will not be taken until the requirement is met.

### 5.0.1. Temperature measurement requirements

DYNAMX measures only temperatures, and the rate of change of the temperatures of each of the probes, in response to a very well controlled heat flow configuration. Hence all of the science requirements on temperature measurement center on achieving the required precision and accuracy in measuring temperature, or rates of temperature change. Since our most demanding science objective is the measurement of $\kappa$ to 5% accuracy in the nonlinear region, the analysis of the science requirements will center on that. Once this objective is achieved, all other objectives are readily achievable.

As discussed in Section 2.3, the thermal conductivity $\kappa$ is determined from Q, the interface advance rate $v_I$, and the rate of temperature change measured at the probe $dT/d\tau$: $\kappa = -Q/(dT/dz) = -Q(dz/d\tau)/(dT/d\tau) = -Q \; v_I \, / \, (dT/d\tau)$. Hence the error $\delta(dT/d\tau) \, / \, dT/d\tau$ creates an equal relative error $\delta\kappa/\kappa$ in the thermal conductivity. The most demanding temperature rate measurement occurs at the lowest Q (10 nW/cm$^2$), where in microgravity and in the middle of the nonliner region, $dT/d\tau$ is estimated to be 12 pK/s based on DYNAMX ground-based data and the simple microgravity model presented in Chapter 2. Hence the cell temperature stability necessary to obtain a 5% measurement of the thermal conductivity in this most demanding situation must be 0.6 pK/s or better. It is important to realize that the experimental challenge becomes easier as T increases past $T_\lambda$, and as Q increases above 10 nW/cm$^2$. For example, for Q = 100 nW/cm$^2$ and at T = $T_\lambda$, we must measure $dT/d\tau$ to within 2 pK/s. All of the science requirements on temperature measurement are designed to assure that these temperature rate measurements may be obtained to this accuracy.

The temperature noise requirement applies to all random temperature fluctuations that may be reduced by averaging. In theory, given enough averaging time, these noise sources may be reduced to zero. In practice, however, a noise requirement must be put in place, since only a finite amount of time is available within a good measurement environment to take the data. An additional requirement, the drift requirement, states the maximum acceptable value of the systematic error in the measurement of $dT/d\tau$ that may never be removed by averaging. The drift rate requirement must be small enough that it will result in no more than one fifth of the total error budget in the thermal conductivity measurements described in the paragraph above. Additionally, the drift rate must create no more than a 0.3 nK change over the 50-minute time interval between determinations of $T_c(Q)$. In addition, the temperature of the probe must be measured to determine its temperature relative to $T_c(Q)$. $T_c(Q)$ and the measurement temperature T are recorded on the same probe, or the difference T - $T_c(Q)$ is determined between different probes. These temperatures must be determined to an accuracy of 1 nK over the course of the scan. As described in Section 5.1.1, the temperature measurement requirement is easily met once the requirement on $dT/d\tau$ is achieved.

The cell temperature measurements must not be adversely affected by charged particle heating, so the stability of the temperature difference between the mini-HRTs and the helium temperature that it measures, referred to as the 'stand-off temperature', must not be greater than 20 nK. This sets a requirement on the total heat flux in or out of the sidewall probes. Additionally, the temperature of the probes must be stable to within the thermometry resolution, setting the requirement on the charged particle heating

fluctuations to the probes, and hence on the total mass on the probe (5g). This requirement on the level of charged particle heating is usually less restrictive than the interface advance rate control requirement, as discussed below.

### 5.0.2. Heat flux control requirement

As discussed in Section 2.2.2, the thermal conductivity is determined from Q, the interface advance rate $v_I$, and the rate of temperature change measured at the probe by $\kappa = -Q/(dT/dz) = -Q(dz/d\tau)/(dT/d\tau) = -Q\ v_I\ /\ (dT/d\tau)$. Hence an error in either the heat flux Q or $v_I$ will create a proportionate error in the thermal conductivity. The quasi-static approximation for $v_I$ is proportional to $\Delta Q$, so an error in $\Delta Q$ creates a proportionate error in $\kappa$. The measurement of $\kappa$ to within 5% between $T_\lambda$ and $T_{nl}(Q)$ places the most restrictive requirements on the heat flux stability. Once this heat flux stability requirement is met, then all other science requirements influenced by heating variations will also be satisfied.

The absolute value of the heat flux through the cell must be known to within a 1% accuracy over the measurement range above each sidewall probe. The accuracy requirement assures that heat flux uncertainties make up 1% out of the 5% total measurement error allowed in $\kappa$ between $T_\lambda$ and $T_{nl}(Q)$. In addition, a much more demanding requirement exists to assure that the interface advance rate remains adequately stable over the course of a ten-minute measurement scan. To achieve no more than a 2.5% uncertainty in the interface velocity, $\Delta Q$ must not vary by more than 2.5% of its set value over any ten-minute scan. Here Q is assumed symbolically to be absolutely stable, so that any instability appears in $\Delta Q$ alone. This uncertainty then will become the largest individual uncertainty in the error budget that assures a measurement of the nonlinear thermal conductivity at the level of 5% in the temperature range of $T_\lambda < T < T_{nl}(Q)$. Assuming the cell cross-sectional area is 4 cm$^2$, and the minimum heat flux in our primary measurement range is 10 nW/cm$^2$, then the total applied heat at our lowest value of Q is simply equal to QA = 40,000 pW. In order to assure a quasi-static interface advance rate over our full measurement range, we require $\Delta Q$ to be less than or equal to 2.0% of Q. Hence the minimum value of the applied excess heat to the warm end of the cell is 0.020 QA = 800 pW. In order to assure that no more than a 2.5% error is made in the interface position, and therefore in the thermal conductivity calculations, it is necessary to hold $\Delta Q$ constant over the 10-minute scan period to within 2.5%. The heat applied to the cell must then be stable to the level of 20 pW over 10 minutes at our smallest Q. The interface advance rate requirement on the maximum acceptable level of heating variation will increase in proportion to Q.

The stray heat requirement discussed above only considers variations in the heat that is applied to the cell warm end for illustrative purposes. Since the cell is cooled through a constant thermal resistance across a constant offset temperature between the cooling stage and the cell cool end, stray heat deposited anywhere on the cell will affect the interface advance rate in the same manner. For example, the relevant mass for the charged-particle stray heat calculations is the mass of the entire cell (30 g). Since the stray heat affects the interface advance rate without regard for where in the cell assembly the heat is deposited, there is no advantage to balancing the mass distribution on each side of the cell.

### 5.0.3. Pressure stability requirements

The DYNAMX experiment will be conducted very close to the 'triple point' where the He-I, He-II, and vapor phases are in coexistence within the cell assembly during data taking. Hence the cell will be maintained at saturated vapor pressure, which is $5 \times 10^3$ Pa. In order to maintain $T_\lambda$ stable to within 0.1 nK, the required pressure stability is one millipascal (1 mPa), which is 0.1 nK multiplied by the slope of the lambda line.

In microgravity the He-I phase will advance into the He-II phase without any appreciable change in the He-II phase temperature, unlike on Earth. Hence the pressure stability requirement may be met by placing a helium bubble in a chamber on the cool end of the cell. The bubble will remain isothermal with the He-II phase throughout the experiment, assuring that the vapor pressure within the bubble remains constant throughout a scan. The vapor bubble must be at least two millimeters in diameter to keep the Young-LaPlace pressure change less than one mPa. The Young-Laplace pressure change results from the increase in the bubble's diameter that arises due to the thermal contraction of the liquid helium during the He-I phase advance.

In addition to basic pressure stability, vibrations create local pressure oscillations that dither the local value of $T_\lambda$, potentially creating a systematic error in the thermal transport measurements. This pressure effect on $T_\lambda$ is used along with vibration induced heating to arrive at the vibration requirement on DYNAMX, as discussed in Section 5.3.1.1.

### 5.0.4. Timing accuracy requirement

A time stamp accuracy of 100 ms is required in order to reconstruct the thermal profiles, and to remove spikes from charged particles that strike the mini-HRTs directly. As a goal, it is desirable to achieve a time stamp accuracy of 10 ms, since that is twice as fast as the demonstrated time constant of the mini-HRTs (20 ms). This required time stamp performance is readily achieved through the planned ethernet link.

### 5.1. Thermometry Requirements

### 5.1.1. Temperature noise requirement

In order to meet the overall cell temperature stability requirements in Section 5.0.1, the mini-HRT noise must not exceed 0.3 nK per root-Hz. The noise spectrum must be random in origin between 0.01 Hz and 10 Hz so that averaging from run to run will result in a reduction of the data noise. As discussed in Chapter 2, the temperature span of the nonlinear region divided by the local temperature gradient sets the spatial width of the nonlinear region. We intend to make at least ten distinct measurements across the nonlinear region. At the highest Q (100 nW/cm$^2$) the maximum distance that the interface may move as each distinct measurement is made is $5 \times 10^{-4}$ cm, which corresponds to an averaging time of 25 seconds as the interface passes the probe closest to the warm endplate. The data averaging of 0.3 nK per root-Hz noise over the 25 second time interval corresponds to an averaged temperature noise of 24 pK. The averaged

temperature noise, divided by the time interval (25 s), results in a noise level in dT/dτ of 1 pK/s, which is half of the required level stated in Section 5.0.1 for Q = 100 nW/cm$^2$. At the opposite end of the heat flux range, 10 nW/cm$^2$, the predicted resolution in dT/dτ is roughly the same (about 1 pK/s). Now, however, the required noise level must be about 0.3 pK/s in order to obtain the same safety margin in the error budget to make a 5% measurement of κ. The required noise level for Q = 10nW/cm$^2$ will be met by averaging similar data scans.

### 5.1.2. Drift requirement

The drift of the mini-HRTs must not exceed $10^{-13}$ K/s (0.1 pK/s). This requirement is driven by two concerns. First, the drift of the HRTs must not exceed 0.1 pK/s so that there is no more than a 0.3 nK change (which is the thermometer noise requirement) over the maximum time interval of 50 minutes between determinations of $T_c(Q)$. Since the determination of $T_c(Q)$ requires up to 5 minutes, and since the time required to travel between equatorial crossings on low-Earth orbit is 45 minutes, the requirement permits all thermometry drift to be tracked accurately through the $T_c(Q)$ determinations. The drift requirement will also assure that $T_c(Q)$ determined at every value of Q will contribute to the total $T_c(Q)$ data set without additional drift corrections. We have observed a long-term drift rate of less than 3 fK/s in the PdMn mini-HRTs that will be used in the flight hardware. The excellent long-term drift performance may degrade to no worse than $2 \times 10^{-14}$ K/s due to short-term drift variations over a fifty-minute measurement period, which still easily meets the science requirement.

Second, the long-term drift rate sets the systematic noise floor on dT/dτ, which must be more stable than 0.3 pK/s to make our most demanding measurement of κ. This drift requirement assures that the thermal conductivity measurements will not be degraded by drift.

### 5.1.3. Time constant requirement

The thermometer must have a time constant faster than one second in order to make accurate measurements of the thermal profiles within the helium at our lowest value of Q (10 nW/cm$^2$) in our primary range of heat flux. A time constant of one second permits the quasi-scaling of the thermal profile to be done accurately, and it does not create a substantial error in the measurement of $T_c(Q)$, or in κ. As a goal we want to achieve a time constant less than 100 ms, since that will permit us to remove the fast thermometer spikes created from direct charged particle hits on the mini-HRTs from the data. By removing spikes from direct charged particle hits we will substantially lower our effective noise level on orbit, as we have demonstrated using Monte-Carlo simulations of such thermometry strikes, and spike removal procedures. Since the helium response time is always long compared to 100 ms, and since the mini-HRT responds with its natural time constant once it is struck, the time constant goal will assure that no noise from charged-particle strikes ever is mistaken for actual helium physics data. In practice, these mini-HRTs have demonstrated a time constant of 20 ms, significantly out-performing the goal.

### 5.1.4.  Thermometer mass requirement

In order to avoid undue restrictions on the maximum variation of charged particle heating, which in turn would greatly limit the time available for on-orbit data taking, the total mass of the mini-HRT must not exceed 4 g.  Since the total mass on the sidewall probe must not exceed 5 g, the mass of the probe foil and its joint to the mini-HRT may have a mass of up to 1 g.  The mini-HRT mass requirement assures that the total mass of the three mini-HRTs on the cell will contribute no more than 12 g to the total cell mass budget of 30 g, as described in Section 5.0.2 above.  The mass of the PdMn thermometer in the DYNAMX prototype is 2.7 g, providing a mass margin on the sidewall probe.

### 5.1.5.  High-resolution thermometry, ground performance

We have developed and tested four different high-resolution thermometers (HRT) for use in association with DYNAMX.  The first thermometer was very close in design to the LPE HRT, with a total mass of 56 g and a copper ammonium bromide (CAB) thermometric element.  While the LPE thermometer was clearly too massive to meet our science requirements, it served as a reference standard against which the other thermometers were compared.  The second was a 'holder' design that isolated the CAB from its niobium flux tube through a vespel [42] cantilever, thereby making its effective mass for charged particle stray heat concerns equal to the mass of the CAB element and the attachment to the stage being measured.  The third was a miniature version of the LPE thermometer, which used a $GdCl_3$ element.  Finally, we developed a miniature HRT with a new thermometric element consisting of 0.7% of Mn in a pure Pd matrix [32].  All of these thermometers displayed excellent noise and drift performance, with the exception of the holder HRT, which was highly microphonic, and the miniature $GdCl_3$ thermometer that displayed a large drift rate of about 10 pK/s.   Of these four thermometers, the PdMn mini-HRT met all of science requirements discussed above with a significant safety margin, and hence has been selected for DYNAMX.  The DYNAMX mini-HRT has demonstrated a noise level of 0.10 nK in a one-hertz bandwidth, with a long-term drift rate of 3 fK/s, and an internal time constant of 20 ms. The effective mini-HRT time constant, in response to helium temperature changes, was 48 ms due to the Kapitza resistance between the thermometry stage and the helium.

The PdMn mini-HRT offers many practical advantages over thermometers that use salts, such as CAB and $GdCl_3$.  There is no risk of damaging the PdMn element through dehydration during fabrication and testing.  Since the PdMn is a stable metallic alloy that melts at 1550 $^o$C, these thermometric elements may be directly brazed and soldered to other metals, greatly improving thermal contact.  The PdMn may be readily machined and sputtered into thin films to create bolometers and other high-speed thermometers.
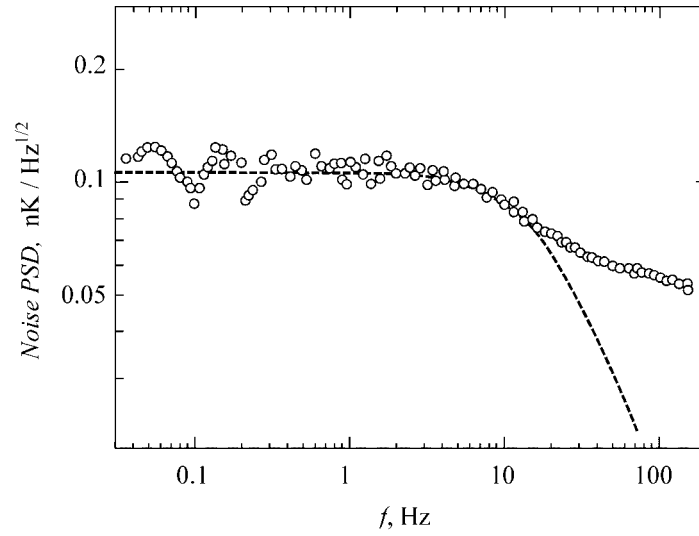
**Figure 18**: The power spectral density of thermal noise from a typical mini-HRT in the flight prototype hardware. The noise level in a one Hz bandwidth is 0.10 nK. The dashed line represents the calculated thermal noise power spectrum density in accord with [32], the time constant of the thermometer $\tau \approx 20$ ms used as a fit parameter.
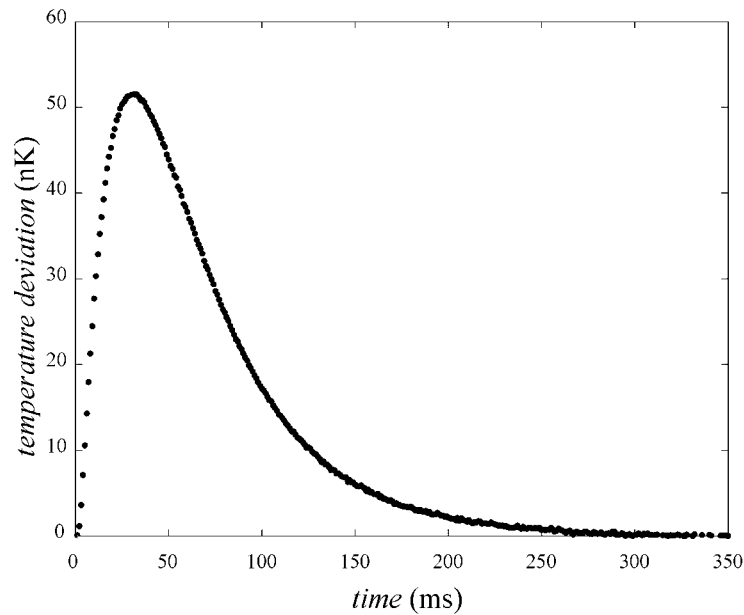


**Figure 19**: The response time of a typical mini-HRT used in the flight prototype hardware. A one millisecond heat pulse was applied to the mini-HRT probe foil, creating a rise time of 20 ms. The characteristic fall time was 48 ms, due primarily to the Kapitza resistance between the probe and the helium.

36

## 5.2. Precision Heater Requirements

### 5.2.1. Cell endplate precision heaters

As stated in Section 5.0.2, the variation in all heat sources to the cell must be less than 20 pW throughout the scan. In order to provide additional error budget for any unexpected heating sources, we require that each of the two high-resolution heaters on the cell have a drift stability of 3 pW or better over the 10-minute scan interval.

In addition to these heater stability requirements, the precision heaters must have a readout and set-point accuracy of 10 pW, with a goal of 1 pW. The absolute accuracy of each heater output must be 1% of the set value over the primary heat flux range. The time constant of each high-precision heater and its associated bias electronics, when attached to the empty cell assembly, must be less than 0.1 second to assure fast settling prior to data taking.

These requirements have been met in the ground-based laboratory many times, and the aerospace industry has indicated that such a requirement can be met using their existing flight electronics in isolation. There is a concern, however, that additional work during the flight hardware development may be required to achieve an adequately low level of electromagnetic interference (EMI) and signal line cross-talk to meet the requirement on the ISS. Methods of EMI reduction and cross-talk suppression will be developed during the engineering/build phases of the flight hardware development.

### 5.2.2. Sidewall probe heaters

These heaters are not required for the on-orbit measurements, however they are necessary for the ground testing and calibration of the ISP before flight. Resistors and leads must be supplied that meet these requirements. Ground support equipment will operate and perform tests with these heaters prior to, and following, the delivery of the ISP to JPL for integration into the flight instrument. These heaters will be used to determine the actual thermal resistance between each thermometer and the liquid helium at many times during the integration and testing. They will also be used to determine the Kapitza resistance between the probes and the helium following the final cool-down prior to launch.

Each of the sidewall probes shall have a heater and an associated driver that can create a heat flux of up to 50 nW/cm$^2$ through the interface between the sidewall thermometer foil and the helium. It should be adjustable in steps of 0.025 nW/cm$^2$, and it should have an absolute accuracy of 0.1 nW/cm$^2$ or better over its full range. The heater will be used to determine the Kapitza resistance between the probe and the helium following environmental tests, and it will be used to calibrate the level of stray heat that is entering or leaving the cell through the sidewall probe. These sidewall heaters must exhibit no more than 0.5 pW of absolute power variation over a 10 minute scan when they are disconnected from their control electronics in the flight environment.

## 5.3. Stray Heat Requirements

### 5.3.1 ISS environment

There exist two major environmental sources of stray heating, namely charged particle heating and stray heating induced by vibrations. The anticipated charged particle heating environment on the ISS orbit is described in Chapter 6. That description, and a numerical model of the heating from charged particles, is based on data from LPE, the APEX satellite experiment, and results from the CREME96 suite of space radiation envrionment codes. The vibration environment has been estimated within the SRED, based on publications from Johnson Space Center staff.

As discussed in Section 5.0.2, the variation in charged particle heating must be stable to within 10 pW over a ten-minute scan at our lowest value of Q (10 nW/cm$^2$). This requirement relaxes in proportion to Q. From our best estimate of the charged particle heating, we have estimated the number of time intervals of ten-minute or greater duration during which the charged-particle heating variation will be sufficiently low to take data at a given Q. We conclude that approximately one half to one third of our time on the ISS will be available for data taking, considering charged particle heating stability alone. A third-time duty cycle for data taking is adequate for our proposed measurements, as described in the Mission Time Line discussion in Chapter 6.

Vibration-induced heating must be maintained at a very low level during the measurements scans. The negative thermal expansion coefficient provides a cooling effect during adiabatic compression which is in the same direction as the pressure shift in $T_\lambda$, substantially reducing the effect of vibrations on the distance of the helium from criticality. Direct measurements of vibration-induced heating indicate that there will be no substantial concern, provided that there are no low-frequency resonances of the DYNAMX ISP structure. An aerospace contractor (SWALES) has recently completed a modal analysis of the DYNAMX ISP, and they estimate that the first structural resonance will occur at 173 Hz. This first resonance frequency has been measured at 134 Hz in the preliminary results from a recent launch-load shake test of our prototype flight hardware. Hence the vibration environment on the ISS, while greater than that experienced on Earth, is not expected to be a major concern.

The environmental requirements below act to define those time intervals on the ISS during which science data may be taken. Data will not be taken during times when any environmental requirement is exceeded. The mission timeline in Chapter 6 estimates the rate of data acquisition, given the anticipated number of ten minute scan intervals that occur with all environmental requirements met.

### 5.3.1.1. Vibration requirement

There are two primary concerns that drive the vibration requirement. First, random vibrations will create stray heat and DYNAMX is sensitive to very low-level changes in stray heat. Second, heat transport near the superfluid helium is affected by pressure changes primarily through the pressure sensitivity of $T_\lambda$ [27], and local temperature changes resulting from adiabatic compression. While the first concern may be addressed on Earth, the second concern will be sensitive to the effects of steady gravity, and must

be estimated within the microgravity environment based on our best understanding of the lambda transition.

Measurements have been made to determine the level of vibrational heating as measured at the sidewall thermometry probes in each of our major cool-downs. These measurements were made with a fully functional apparatus, and science data were taken under low-level shake and compared to similar data taken without shaking. The applied shake did not influence the experimental data in any detectable way at shake amplitudes up to 1 mg$_{rms}$, and at shake frequencies up to 100 Hz, provided that the shake frequency was de-tuned from the structural resonance of the probe. At a structural resonance, however, the level of stray heating dramatically exceeded science requirements. In an earlier cell constructed of vespel [42] sidewalls, no observable dissipation was observed from 10 - 50 Hz. Vibrational heating was observed above 50 Hz, which was associated with a structural resonance at 85 Hz. The maximum vibrational heating on resonance using a 0.5 mg$_{rms}$ drive level at a sidewall probe was 2.06 nW, which resulted in a steady state temperature rise of 112 nK. The maximum vibrational stray heat increased to 11.2 nW on resonance when the drive level was increased to 1 mg$_{rms}$. The stray heat was determined by multiplying the observed shake-induced temperature rise by the effective resistance between the probe and the isothermal superfluid helium. The effective probe thermal resistance to the helium was determined by a separate, direct measurement, using a precision heater mounted on the thermometry stage.

The second concern, namely the effect of vibration-induced pressure variations that modify the heat transport in liquid $^4$He directly, has been the focus of further study and a separate experimental measurement. When the acceleration changes by an amount $\Delta$g, the pressure change $\Delta$P at a depth h in the liquid helium of density $\rho$ is simply

$$\Delta P = \rho h \Delta g \cdot$$

Due to the pressure dependence of $T_\lambda$,

$$\Delta T_\lambda = \alpha \Delta P = \alpha \rho h \Delta g \cdot$$

Numerically, $\alpha$ = -88.5 nK/Pa, which is the slope of the lambda line, and $\alpha \rho h$ = -129 nKs$^2$/m, assuming that h = 1 cm, which is typical for our cell. Hence, in the He-I phase, a positive $\Delta$g will act to move the $^4$He further from criticality.

Fortunately, a second pressure effect tends to lessen this pressure-induced departure from criticality. Since the isobaric thermal expansion coefficient is negative near $T_\lambda$ , the $^4$He liquid becomes more dense when its temperature increases. Hence, when the pressure change in the liquid $^4$He occurs adiabatically, the density of the $^4$He increases and the temperature goes down. This temperature change is

$$\Delta T = -\beta \Delta P = -\beta \rho h \Delta g,$$

Numerically, $\beta$ = 64 nK/Pa and -$\beta \rho h$ = -93 nKs$^2$/m, again assuming that h = 1 cm.

This results in a change in the distance from criticality given by:

$$\Delta t = (\Delta T - \Delta T_\lambda)/T_\lambda.$$

Since $\Delta T$ and $\Delta T_\lambda$ are in the same direction in response to some stray acceleration $\Delta g$, the departure from criticality is relatively small. Specifically,

$$\Delta t = 1.65 \times 10^{-8} \ s^2/m \ \Delta g.$$

Hence if $\Delta g = 10^{-2} \ m/s^2$ (one 'milli-g'), then the variation in $\Delta t$ would be only about $1.7 \times 10^{-10}$, which is approximately equal to the minimum resolvable change in $\Delta t$ based on our thermometry noise.

The adiabatic cooling effect was measured directly in a brief experiment at JPL, which is documented in DX-DF-133. The pressure on a liquid helium sample in its He-II phase near $T_\lambda$ is suddenly increased by 110 Pa, and the cell temperature deceased by 6.0 $\mu K$. The experimental value of $\beta$ is 50 nK/Pa, which is slightly smaller than the theoretical estimate above. Using the experimental value, along with the pressure effect on $T_\lambda$, the departure of the system from criticality $\Delta t$ is anticipated to be

$$\Delta t = 2.5 \times 10^{-8} \ s^2/m \ \Delta g.$$

As discussed in Chapter 2, the thermal conductivity, $\kappa$, of $^4He$ near $T_\lambda$ diverges roughly as $\kappa \sim t^{-0.39}$, and hence the heat transport is exceptionally sensitive to changes in t. Since the thermal conductivity, $\kappa$, varies in a non-linear way with t, and hence also with $\Delta P$ and $\Delta g$, the error in $\kappa$ was estimated in the presence of $\Delta g$, using our ground-based experimental data for the variation of $\kappa$ on t. If the vibration frequency that creates $\Delta g$ is much higher than the 10 Hz bandwidth of our high-resolution thermometers, then there is no direct way to correlate the vibration induced measurement error to the source of the vibration. These estimates of the error in $\kappa$ due to vibrations above the measurement bandwidth must remain less than 1%, which is 1/5 of our total error budget for thermal conductivity measurements in the range $T_\lambda \le T \le T_{nl}(Q)$. This sets the requirement on the maximum value of $\Delta g$ above the measurement bandwidth, which was found to be 0.5 $mg_{rms}$ for all frequencies greater than 10 Hz.

For frequencies less than 10 Hz the vibration induced errors may be directly correlated with independent, time-stamped, measurements of the vibration level. Such a procedure is important, since low-frequency acceleration noise can not be attenuated effectively by any passive or active vibration isolation system. Hence the actual vibration noise at low frequencies will be monitored using the SAMS system or an equivalent method of monitoring the ISS vibrations at the experiment. Real-time vibration data at low-frequencies will permit experimental corrections to be applied, and/or permit the veto of data during intervals of unusually high low-frequency noise.

### 5.3.1.2. Steady acceleration requirement

Any steady acceleration during the DYNAMX experiment must be less than 31 µg. An acceleration of 31 µg directed perpendicular to the axis of the DYNAMX cell would create a variation of 0.1 nK in $T_\lambda$ across the diameter of the cell. Such a variation would be barely detectable experimentally, given the DYNAMX thermometry noise level. By the same condition, a steady acceleration of 86 µg could be tolerated, provided that this steady acceleration is aligned with the axis of the cell. Since the steady acceleration is predicted to be about 3 µg at the LTMPF location on the ISS, residual acceleration is not expected to be a concern for DYNAMX, and no special orientation with respect to the residual acceleration is required.

### 5.3.1.3 Charged particle environment

The most stringent requirement on the charged-particle heating is set at our smallest value of Q, 10 nW/cm$^2$. At that low Q the stability of all heat sources applied to the cell must not vary by more than 20 pW over a ten-minute scan period, as described in Section 5.0.2. Allowing up to half of the stray heat variation to come from the variation of the charged-particle heating sets a requirement that the variation of the charged-particle heating of the cell must be less than 10 pW over a minimum of 10 minutes. We show in Section 6 that this requirement will be met.

### 5.3.2. Instrument Guard Vacuum Requirement

The residual pressure in the Instrument Guard Vacuum (IGV) that surrounds the ISP must not exceed one micropascal (1 µPa). Such good vacuum is necessary to control stray heat, and to keep heat conduction paths that run parallel to the cell at an absolute minimum. The maximum heat flow through the residual gas in the Instrument Guard Vacuum (IGV) must not change the temperature indication of a sidewall probe by more than 0.1 nK. The effective thermal resistance between the thinnest (50 µ) probe and the helium is 50 K/W, so the stray heat through the vacuum to any probe must not exceed 2 pW. Taking estimates from the effective parameters from the ISP design, and the residual heat conduction from residual gas as summarized in White [44], the residual gas pressure in the IGV must not exceed one micropascal (1 µPa), assuming that the inner shield is operated 10 µK above $T_\lambda$. Exchange gas, either $^3$He or $^4$He, may be used within the IGV to cool cryoprobe components during launch, and must be evacuated before data taking. Exchange gas was used successfully on both LPE and CHeX. The IGV residual gas pressure was reduced to less than 0.1 µPa on CHeX using an improved sorb pump. Such a pump will be used on the LTMPF cryoprobe if launch exchange gas is necessary. Hence the DX science requirement on residual IGV pressure will be met.

### 5.3.3. Sidewall probe heat flux requirement

The thermal resistance between the sidewall probes and the helium is the Kapitza resistance, which has been measured at 2 cm$^2$K/W. In order to keep the temperature difference between the probe and the helium adjacent to it at or below 20 nK the sidewall

probe must not create more than a 10 nW/cm$^2$ heat flux into or out of the helium. This requirement is large so that measurements over the extended range of Q may be made in relatively high charged particle heating environments, provided that this heat flux is steady over the measurement interval. The goal for this heat flux from the sidewall probe is 2 nW/cm$^2$.

### 5.3.4.        $^3$He impurity requirement

The helium sample $^3$He concentration must not exceed 10 parts $^3$He in 10$^9$ parts of $^4$He (10 ppb), with a goal of 1 ppb. Prof. Peter McClintock has observed clear signatures of $^3$He impurity effects in precision measurements when standard well helium, with about 1,000 ppb $^3$He impurity, is used. The heat flux in our cell will sweep any residual $^3$He impurity to the cold endplate, leaving the remaining cell virtually perfectly pure as long as there is no $^3$He back-diffusion. This requirement assures that impurity effects will not be a problem.

### 5.4.        Preliminary functional requirements

We have developed and tested a flight prototype instrument that is designed to simultaneously meet the science requirements in an apparatus that is likely to survive flight. Only the preliminary functional requirements that are relevant to the cell construction and design are discussed here. Many other functional requirements have been determined, and they will be presented in the Functional Requirements Document (FRD), which will be reviewed at the Critical Design Review.

### 5.4.1.  Cell specifications

### 5.4.1.1. Cell geometry

The optimal cell diameter is 2.5 cm. Larger cell diameters are more sensitive to vibration and stray steady acceleration. As the cell becomes smaller its total heat capacity decreases, making the cell temperature more susceptible to stray heating effects.

### 5.4.1.2. Cell construction material

The cell endplates must be constructed using aluminum, or a less dense metal, to avoid excessive charged particle heating. These endplates must have a thermal conductivity of at least 1 W/(cm K), with a goal of 10 W/(cm K). The cell sidewall must be constructed from an insulating material with a thermal conductivity below 1.5 mW/(cm K). The sidewall thickness must not exceed 100 μ to assure that sidewall heating does not adversely affect the measurements. Finally, the sidewall thickness must be uniform to within 10 μ around its circumference and along its length to assure that the sidewall stray heat is uniform to within 10%.

### 5.4.2. Sidewall probe specifications

The sidewall thermometry probes must each provide a uniform temperature sampling around its full circumference, with no more than a 5% variation in the heat flux to/from the probe around the full circumference of the probe, with a goal of 1%. A uniform heat sampling around the circumference will assure that the maximum variation in the heat flowing from or to the sidewall probe will be uniform around the probe, preserving the cylindrical symmetry of the cell. Since the entire surface area of the probe participates in the heat conduction, the resistance between the helium and the mini-HRTs will be minimized, lowering the noise of the thermometers and decreasing their time constants.

The sidewall uniformity requirement has been met by increasing the probe thickness to the maximum possible extent, and by achieving a residual resistance ratio (RRR) of at least 1,000 in the probe copper, which corresponds to a thermal conductivity of over 50 W/cmK. The probe RRR is typically 2,000 following our vacuum and oxygen annealing, which may decrease to no less than 1,500 following post-anneal handling. Thermal simulations, along with measurements of the Kapitza resistance between the probes and the helium, and measurements of the copper conductivity of the probes, confirm that the required probe temperature uniformity is achieved in our current cell designs. For probe thickness less than 75 μ, a 125 μ thick copper annulus is soldered onto the probe foil just outside the diameter of the cell to assure such sampling uniformity.

The probe must be thin enough to assure that it does not smear out the thermal gradient to be measured. Smearing is most relevant when the interface moves past the probe. The spatial extent of the interface is expected to be about 300 μm, so the probe should not be greater than one-half of the interfacial thickness. The effects of the systematic error introduced from the probe's averaging of the thermal gradient has been calculated analytically and checked experimentally. The probe thickness must be as large as possible for the following two reasons: A thicker probe provides a lower total resistance between the liquid helium and the thermometer, and hence results in a lower noise level. Secondly, a thicker probe permits greater variation in the level of charged particle heating absorbed by the associated thermometer over the measurement interval, permitting a greater mini-HRT mass. At a given thermometer mass, a thicker probe makes it possible to increase the data taking time on orbit by permitting a wider variation in the charged particle heating before the science requirements on probe stray heat are violated.

From these considerations, the ideal probe thickness is 75 μ, which has been achieved and used experimentally in ground-based measurements. Furthermore, two other less optimal probes of 50 μ and 125 μ thickness will also be used on orbit. Such a distribution of probes will permit a confirmation during on-orbit data taking that the probe thickness is not introducing an uncontrolled systematic error in the measurements. We have used probes of five different thickness in our ground-based measurements, and we have used probes of two different thickness to confirm that our data, following the systematic sidewall corrections described in Chapter 2, show no dependence on the probe thickness.

The first sidewall probe is located at 5.0 mm from the heated endplate in order to assure that an adequate normal fluid buffer exists to protect the interface advance from

random stray heat fluctuations. The second probe is located 1.0 mm above the first, and the third probe is located 1.0 mm above the second. The cool endplate is located 2.0 mm above the third probe. The distances above should be within 10% of the stated values, and the actual position of each probe relative to the two endplates must be determined to within 10 μ following the probe sidewall fabrication. A certainty of each probe's position to within 10 μ will assure that dimensional uncertainty does not appreciably affect the error budget on the heat transport measurement objectives. Such a level of measurement accuracy has been achieved in our ground-based work, and may be improved in future cell inspections through the use of commercial coordinate measuring machines (CMM).

# 6.        Flight Experiment Plan

The basic measurement procedure is outlined here, along with a time line of the actual measurements aboard the orbiting laboratory.

## 6.1 Experimental procedure

There are three major procedures that will be followed throughout the course of the orbiting experiment.  They are the 1) Initial Power-Up and Stabilization Routine, 2) Calibration and Test Routine, and 3) Measurement Routine.

The Initial Power-Up Routine will be applied once at the beginning of the experiment, unless an unexpected loss of power or other outage in encountered during the mission.  Once the experiment is powered up within the LTMPF facility it will be at or below a temperature of 2.0 K.  All heater controllers will be set to dissipate no heat initially, and all the bridges and high-resolution thermometers will be activated.  An initial 'status-of-health' check will be made to assure that all rough thermometry indications are consistent, that all heaters, servo controllers, and HRT readout circuits are responding properly, and that all environmental indicators, such as charged particle counters, residual gas pressure indicators, and helium level indicators are as expected.  Then the cryoprobe will establish operational servos on all its stages, including the stage that cools the ISP.  Once the servos are operational and the ISP has come to thermal equilibrium with the isothermal platform of the cryoprobe, the indicated temperatures on all the ISP stages will be compared to the set temperature of the isothermal platform.  Once the comparison has been made the cell cooling stage will be brought to its designed operating temperature for a heat flux of 100 nW/cm$^2$.  The functionality of all other heaters, thermometers, and servo systems will be checked at this time.

The Calibration and Test Routine will calibrate all the thermometers within the ISP against a standard thermometer, which will be mounted on the cell cool endplate, over the calibration range of fifty microkelvins on either side of $T_\lambda$.  The standard thermometer may be a calibrated GRT, or a thermometer of more rugged construction that is less likely to be adversely affected by launch and the space flight environment.  The value of $T_\lambda$ will be determined to within 100 nK during the calibration procedure by making fast measurements of the heat capacity of the cell.  These heat capacity measurements will be achieved by pulsing the cell heater and noting the resulting temperature rise of the cell with the cooling stage temperature held constant at roughly the initial cell temperature.  The fast heat capacity measurement will also be used as a check of the thermometry calibration near $T_\lambda$.  The Calibration and Test Routine will be repeated at least twice over the course of the measurements, and more often if necessary.  A final calibration will be performed just prior to the loss of cryogen, or the termination of the DYNAMX experiment.

All of the measurements to be performed on orbit during the Measurement Routine consist of the following three steps:

1) The cell is placed in its He-II phase and approximately 25 nK below $T_\lambda$ when the measurement procedure begins.  A total of twice the total required heat to create the maximum value of Q (100 nW/cm$^2$ in the primary range of Q) will be dissipated on the cell, with half on the cell cool endplate, and half on the cell

warm end.  As the heat is increased slowly, the set-point of the cooling stage will be lowered to keep the helium roughly isothermal.  Then the heat will be decreased on the warm end of the cell in order to achieve the desired heat flux Q for the upcoming measurement, with a corresponding increase in the heat at the cell cool end in order to maintain the cell isothermal without changing the cooling stage's temperature.  Finally, once the cell has settled to steady state, additional heat will be applied to the cell warm end plate to create the desired $\Delta Q$.  The cell is then permitted to drift until the interface appears and enters the cell.  The temperatures, as the interface advances by each thermometry stage, are digitized and transmitted to Earth at a rate of at least 1 kHz.

2)  In order to check for hysteresis, the power dissipated on the cell warm end is decreased by twice the amount of the initial increase that was used to create the $\Delta Q$.  The interface advance rate then reverses, and any difference in the temperatures at which the interface entered the cell, and when it leaves, will be recorded.

3)  In order to measure the thermal profiles, the interface will be permitted to sweep past at least two of the three thermometry probes.  Once the scan is complete the interface position will be reset to either its 'parked' position 25 nK below $T_c(Q)$, or at its 'standby' position at about 1 mm below the thermometry probe.  All adjustments in Q will occur with the interface in the 'parked' position. All data on the thermal profile and the thermal conductivity measurements will be obtained through the use of the third procedure.

Occasionally the interface will be maintained in its parked position with zero applied heat flux in order to measure the variation in the charged particle heating rate around the orbit.  In this mode the cell is simply being used as a charged particle calorimeter.

**6.2 Mission Timeline**

The accuracy of DYNAMX measurements can be affected by the charged-particle heating from the space radiation environment, as described in Sections 5.0.1 and 5.0.2. To address this issue we have carefully considered the charged-particle heating environment at the ISS orbit and designed a mission timeline which should ensure a 100% science return even in a worst-case scenario.
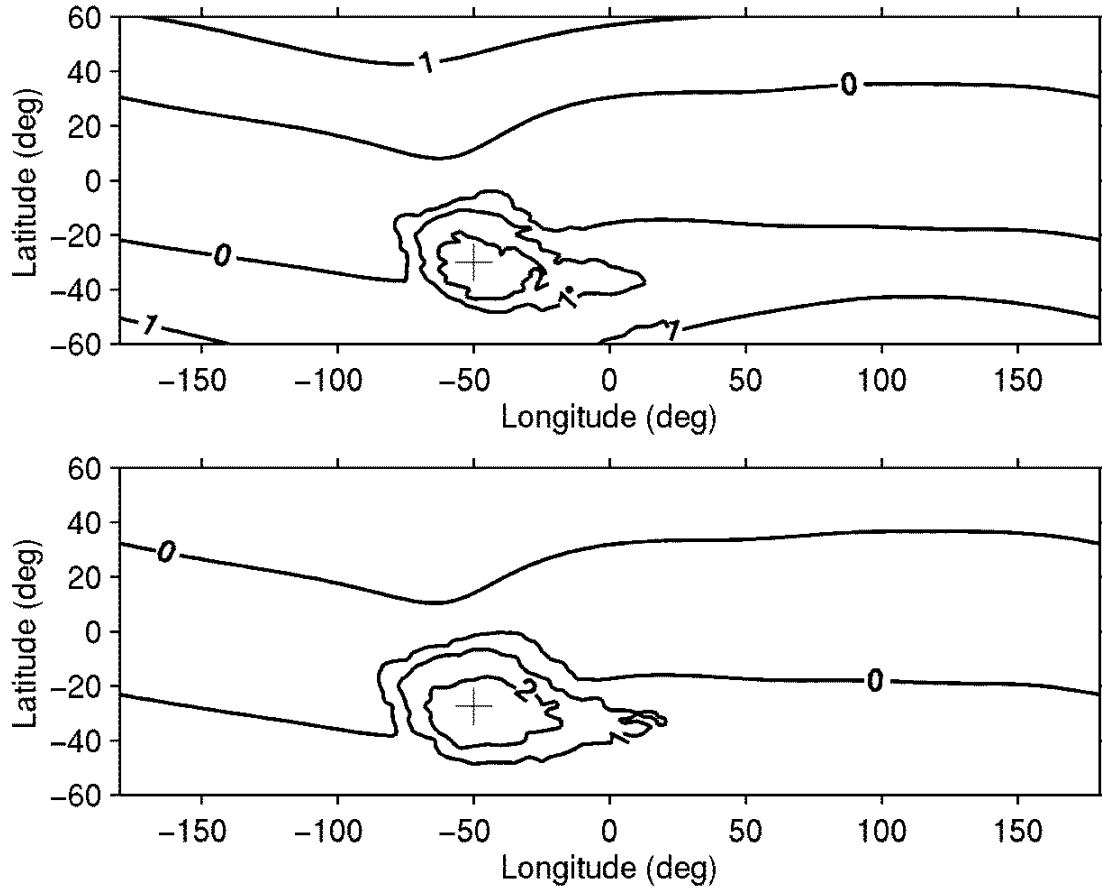
**Figure 20**: Charged-particle heating estimates for ISS orbit. Contours shown are the $\log_{10}$ of the heating in pW/g expected from the galactic cosmic rays and the trapped particles, assuming an effective shielding level similar to that of the Lambda Point Experiment. The space radiation environment is a function of the 11-year solar cycle, and so is the altitude of the ISS, which varies from about 370 km at solar minimum (upper plot) when the Earth's atmosphere is coolest and most contracted, up to about 470 km at solar maximum (lower plot) when the earth's atmosphere is warmest and most expanded. The large heating peak is the "South Atlantic Anomaly", where the ISS orbit passes through the inner boundary of the inner Van Allen radiation belt. The location of the maximum heating in each plot is indicated by the large "+". At solar minimum the maximum heating is about 630 pW/g. At solar maximum the maximum heating is about 560 pW/g.

### 6.2.1. The Space Radiation Environment

The most important feature of the space radiation environment from the point of view of DYNAMX is the bulk heating that will result from the passage of penetrating charged particles through different parts of the experiment. The heating to be seen on the ISS orbit is shown in Figure 20. Plots are shown for both "solar maximum" and "solar minimum" conditions, because both the space radiation environment and the ISS altitude vary as functions of the 11-year solar cycle. This heating estimate is developed from data from the Lambda Point and APEX experiments, and from the CREME96 suite of space radiation environment codes. Details of the development of these estimates are available

at *http://coffee.phys.unm.edu/~stpboyd/space_environment*. In developing these estimates an effective shielding level comparable to that of the Lambda Point Experiment is assumed. In our analysis we neglect the periods of higher heating which are due to solar flares, because these occur infrequently (~ every few months) and are of short duration (~ few days) compared to an ISS mission.

The large peak in the heating over the South Atlantic Ocean is called the "South Atlantic Anomaly" (SAA). This heating peak arises because the geomagnetic dipole of the earth is displaced from the gravitational center of the earth by some hundreds of kilometers toward the north Pacific. Because of this the inner surface of the inner Van Allen radiation belt is eccentric with respect to the circular orbit of the ISS, and the ISS orbit penetrates shallowly into the radiation belt over the South Atlantic. The large flux of lower-energy "trapped particles" inside the radiation belt produces the localized region of high heating which is indicated. Away from the SAA the trapped particle heating is negligible over the rest of the ISS orbit, except at the highest latitudes, where it is thought that a level of heating much smaller than that of the SAA is contributed by the "horns" of the electron distribution.

The much smaller variation in heating seen away from the SAA is caused by "galactic cosmic rays", which are bare atomic nuclei of extrasolar origin. In interplanetary space the flux of galactic cosmic rays is nearly isotropic, but in low-earth orbit the geomagnetic field filters the fluxes according to the ratio of particle momentum to charge. This ratio is called the "rigidity" of the particle. The geomagnetic field acts as a high-pass filter in rigidity, and the "shoulder frequency" of the filter goes to zero at high geomagnetic latitudes and is maximal near the geomagnetic equator, yielding the heating pattern shown.


## 6.2.2 Considerations in Developing a Mission Timeline

### 6.2.2.1 The South Atlantic Anomaly

Passages through the SAA will cause periods of high heating, up to ~600 pW/g, which last for a few minutes. Results in our laboratory indicate the the time constants for re-equilibrating the experiment after such heating are of order one or two minutes. However, to be conservative in the development of the mission timeline, we will not plan to perform any measurements within 30 minutes after any passage close enough to the center of the SAA to produce a heating level greater than 50 pW/g.


### 6.2.2.2 Galactic Cosmic Rays

The relationship of the actual heating to the incident particle fluxes is complicated by the development of secondary showers of particles, both in the experimental apparatus and in distant parts of the space vehicle, which result from nuclear interactions with the galactic cosmic rays. The data from LPE, and possible new data from CHeX, are the only measurements to date of the actual *heating* (rather than *dose rate*) due to the space radiation environment. The model which generated the heating maps shown in Figure 20 was "calibrated" for the conversion from fluxes to heating by comparison to the

calorimetric measurements of the heating caused by the space radiation environment which were obtained as part of the data analysis of the Lambda Point Experiment.

Because the relationship of heating to incident flux is complicated and difficult to accurately calculate, the galactic cosmic ray part of the heating estimates shown in Figure 20 should be considered most reliable in the rigidity range which was directly probed by the Lambda Point Experiment. This range corresponds to a galactic cosmic ray heating level of about 2 pW/g, forming a band centered on the geomagnetic equator. The change in the shape of the galactic cosmic ray spectra as we move farther away from this band will cause a gradual decrease in the accuracy of this estimate, as we move farther away from the spectra directly probed by LPE.

For this reason we consider that the most conservative approach to developing a mission timeline is to plan to do all DYNAMX measurements within the rigidity band which was well-probed by LPE. Because the DYNAMX measurements already comprise a series of many individual temperature sweeps of short duration, this constraint can be included in the mission timeline with no negative impact. The adoption of this conservative stance in mission planning should put to rest any concerns about the ability of DYNAMX to perform in the space radiation environment of the ISS.

**6.2.3 The Mission Timeline**

The required time interval to perform a measurement of the nonlinear region for DYNAMX is 10 minutes. Following the arguments presented in the last section, for a conservative approach we wish to perform those measurements within the equatorial band where heating $\leq 2$ pW/g. Further, we will exclude 30-minute periods after SAA passages. For measurements at lower values of heat flux Q the requirement in the allowable heating variation over the duration of the measurement which was discussed in Section 5.0.2 will also apply.

We need to know how many measurement periods for each value of heat flux Q will be available per day. Using the heating model shown in Figure 20 we can generate heating time series for calculated ISS trajectories. From these heating time series we can calculate the average number of time intervals per day which meet all requirements. These acceptable time intervals we call "measurement intervals".

The orbital tracks of the measurement intervals resulting from two such calculations are shown in Figure 21. The periods between measurement intervals will be used to prepare the cell for the next temperature sweep. The calculated average number of measurement intervals per day for the full range of the primary range of Q is presented in Figure 22.

It is noteworthy that for many of these sweeps we will have measurement intervals which are much longer than the minimum required time of 10 minutes. The mean duration of the measurement intervals over the primary Q range is presented in Figure 23. The extra time available in these measurement intervals will allow us to probe farther away in reduced temperature from the transition, thereby making contact with the linear region that has been explored extensively on Earth.

The minimum science return requirement of DYNAMX is to perform 5 scans at each of twenty values of Q in the primary range of 10-100 nW/cm$^2$, plus an additional 5 scans

to look for hysteresis. Based on the data in Figure 22, the minimum time required for these 105 scans would be a bit more than four days.
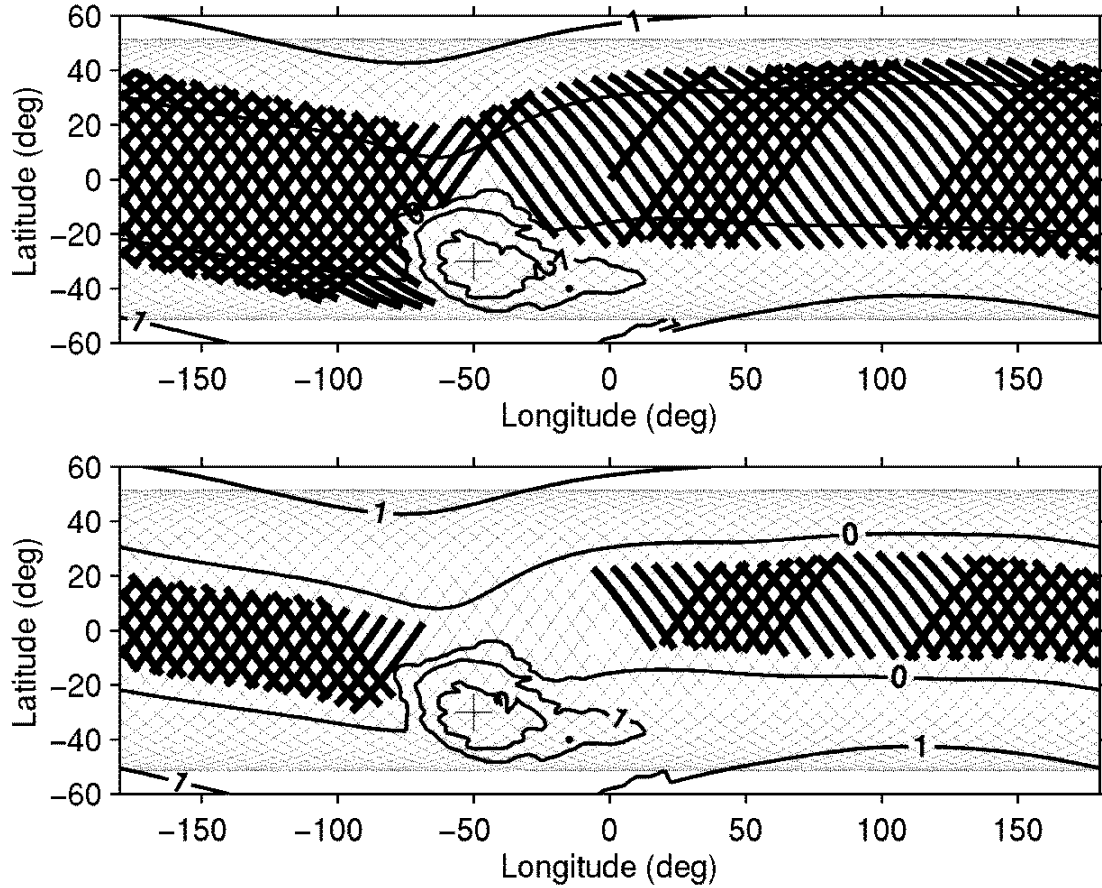


**Figure 21**: Orbital tracks of measurement intervals, superimposed on the charged-particle heating map for solar minimum. Measurement intervals (thickest lines) are selected from a sample 3 day orbital track (thin dashed lines). Solar minimum conditions show the full range of variation of the measurement intervals for different heat fluxes in the primary range of Q. The upper plot shows the orbital tracks of measurement intervals for $Q \geq 55$ nW/cm$^2$, where the measurement intervals completely span the rigidity band probed by LPE (see text for explanation). There are 75 measurement intervals in the 3-day period shown, for an average of 25 measurement intervals per day. The mean duration of the measurement intervals is 22.5 minutes. The lower plot shows the orbital tracks for the measurement intervals for $Q=10$ nW/cm$^2$, the lowest heat flux in the primary range of Q. In this case, as for all $Q < 55$ nW/cm$^2$, the measurement intervals are delimited by the Q-dependent interface advance rate variation requirement. There are 62 measurement intervals in 3 days, for an average of 20.7 measurement intervals per day. The mean duration of the measurement intervals is 11.7 minutes.

The 100% science return requirement adds another 100 scans sampling the extended Q ranges 5-10 nW/cm$^2$ and 100-200 nW/cm$^2$, plus15 more hysteresis scans, to the minimum science return requirement. At $Q=5$ nW/cm$^2$, only 3 measurement intervals are available per day on average at solar minimum. The total time to perform the 100% science return activities, including the time required for the minimum science return activities, would be 11 days.
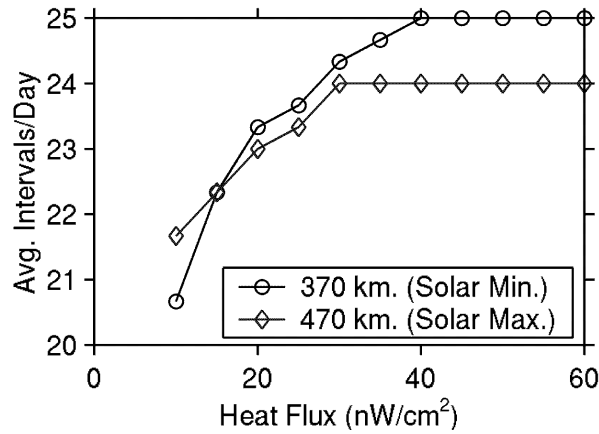
**Figure 22**: Average number of measurement intervals per day for temperature sweeps with different heat flux Q in the lower part of the 10-100 nW/cm$^2$ primary range of Q. Connecting lines are drawn to guide the eye. Results are shown for ISS at Solar Maximum and Solar Minimum, assuming an effective shielding level approximately equivalent to the LPE mission. For Q $\geq$ 40 nW/cm$^2$, the number of measurement intervals per day is delimited by the Q-independent requirement to stay within the LPE rigidity band. Values of Q greater than those shown here simply continue the constant trend to the right. For Q < 40 nW/cm$^2$, the number of intervals per day becomes Q-dependent because the measurement intervals are delimited by the interface advance rate variation requirement. Even at 10 nW/cm$^2$, the lowest value of the extended Q range, the reduction of the number of measurement intervals per day need cause no increase in the required data-taking time. The reduction shown can easily be compensated for by proper choice of heat flux Q and the measurement type (i.e. hysteresis or temperature profile) for each measurement interval during the day.
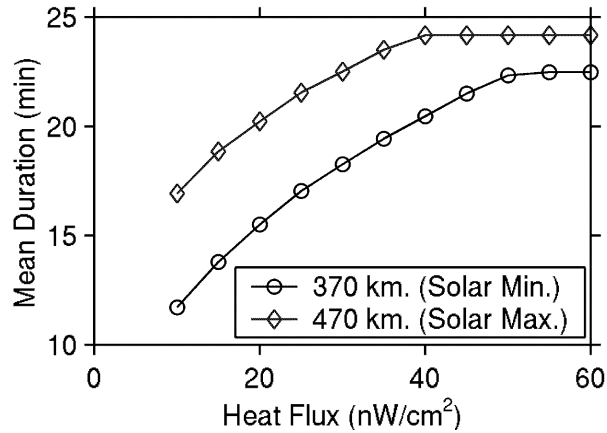


**Figure 23**: The mean duration of the measurement intervals shown in Figure 22. Connecting lines are drawn to guide the eye. For lower Q the average interval length increases with Q because the measurement intervals are delimited by the interface advance rate variation requirement. For Q $\geq$ 55 nW/cm$^2$ the Q-independent LPE rigidity envelope delimits the measurement intervals. Values of Q greater than those shown here simply continue the constant trend to the right.

51

Of course, things never go perfectly smoothly, so we should probably double this estimate of the time required for 100% science return to 22 days. Further, we'll want some period at the beginning of the experiment to do some practice sweeps and to measure charged particle heating to fine-tune our charged-particle heating model. If we allocate an additional 8 days for that activity we end up with a total of 30 days to perform the 100% science return activities.

The ISS is required to provide the microgravity environment in continuous intervals of at least 30 days, and to provide it for a minimum of 180 days per year. If we assume the ISS provides at least 3 periods of 30 days of microgravity during the 6 months of the DYNAMX mission, which seems reasonable, then the total experimentation time available for the mission is about 3X a reasonable estimate for the time required for 100% science return.

If DYNAMX has extra microgravity time available after finishing its 100% science return activities, the experiment will proceed on to the "extra-credit" activities described in Section 6.5.3. In addition to those activities some portion of the extra time may be devoted to additional temperature sweeps at very low values of Q, in the range 1-5 nW/cm$^2$ where measurement intervals are available only rarely.


## 6.3. Facility resource needs

### 6.3.1.        Bandwidth
In order to realize full benefit from the exceptionally fast mini-HRT thermometers the telemetry bandwidth must be at least 1 kHz, with 2 kHz as a goal.

### 6.3.2.        Mass support
The total cryogenic mass requirements to support the DYNAMX ISP is 3.0 kg. No external probe instrumentation is required aside from the two PI-specific boards in the electronics crate.

### 6.4.        Post-flight calibration

The ISP will be returned to the PI for at least three months for post-flight calibration and test. Close-out calibrations will be performed on all the GRT and mini-HRT thermometers, and the thermal isolation between stages will be checked. The experimental cell will be ruptured following the depletion of cryogen, so detailed post-flight cell measurements will not be possible.


### 6.5.        Mission success criterion

### 6.5.1.        100% science return

The 100% science return will consist of five scans at each of twenty values of Q spanning the primary range, along with an equal number of scans in the extended range. In addition, at least 20 scans to search for hysteresis must be conducted.

### 6.5.2. Minimum science return

The minimum science return will consist of five scans at each of twenty values of Q spanning the primary range, and five scans to search for hysteresis. Five scans will permit adequate data averaging to achieve the basic science objectives, however the data sets will not be extensive. While adequate data will be available to answer the basic questions, more data would be required to obtain a 100% science return.

### 6.5.3. Extra-credit

If time permits, following the achievement of a 100% science return, then more data will be taken and averaged in order to reduce the experimental noise further. Also, more detailed studies of the charged particle heating variation on the ISS orbit will be conducted, using the DYNAMX cell as a calorimeter. Finally, any remaining time will be used in collaborations with other Principal Investigators within the Microgravity Fundamental Physics Discipline to obtain initial data that will help define their upcoming flight experiments.

## 7. Prior Published Work

The following papers are selected from our research results that have appeared, or will soon appear, in refereed scientific journals. They include:

1.   R.V. Duncan, D.A. Sergatskov, S.T.P. Boyd, S.S. McCready, T.D. McCarson, A.V. Babkin, P.K. Day, F-C. Liu, and D. Elliott, to appear in *J. Low Temp. Phys*.

2.   R.V. Duncan, P.K. Day, D. Elliott, D.A. Sergatskov, and A. Babkin, to appear in *Physica*.

3.   B.J. Klemme, M.J. Adriaans, P.K. Day, D.A. Sergatskov, T.L. Aselage, and R.V. Duncan, *J. Low Temp. Phys*. **116**, 133 (1999).

4.   P. Day, W. Moeur, S. McCready, D. Sergatskov, and R. Duncan, *Phys. Rev. Lett*., **81,** 2474 (1998).

5.   R.V. Duncan, P.K. Day, S.S. McCready, W.A. Moeur, F-C. Liu, and D.A. Sergatskov, J. Low Temp. Phys. **113**, 861 (1998).

6.   W.A. Moeur, P.K. Day, F-C. Liu, S.T.P. Boyd, M.J. Adriaans, and R.V. Duncan, *Phys. Rev. Lett*., **78,** 2421 (1997).

7.   P. Weichman, A. Prasad, R. Mukhopadhyay, and J. Miller, *Phys. Rev. Lett*., **80,** 22 (1997).

8.   F-C. Liu, R.V. Duncan, U. Israelsson, T. Chui, D. Hensinger, A. Nash, M. Adriaans, and W. Moeur, *Czech. J. Phys. Suppl. S1* **46**, 87 (1996).

# 8. References

1. The only impurity in $^4$He that remains liquid is the isotope $^3$He, which may be reduced in concentration to less than $10^{-12}$ [P.C. Hendry and P.V.E. McClintock, *Cryogenics* **25**, 526 (1985)]. We typically use isotopic purified $^4$He with a residual atomic concentration of $^3$He of less than $8 \times 10^{-10}$. During our measurements, even our lowest value of Q will heat-flush [R.P. Behringer, *J. Low Temp. Phys.* **62**, 15 (1986)] this residual $^3$He to the cold endplate of the cell, and hence out of the measurement region between the sidewall probes. This low $^3$He concentration is far too sparse to form a monolayer on the cold endplate.

2. V. L. Ginzburg and A.A. Sobyanin, *Phys. Lett.* **69A**, 417 (1979); *J. Low Temp. Phys.* **49**, 507 (1982).

3. J. A. Lipa, D. R. Swanson, J.A. Nissen, T.C.P. Chui, and U.E. Israelsson, *Phys. Rev. Lett.* **76**, 944 (1996).

4. J. A. Lipa, D. R. Swanson, J.A. Nissen, P.R. Williamson, K. Geng, D.A. Stricker, T.C.P. Chui, U.E. Israelson, and M. Larson, *J. Low Temp. Phys.* **113**, 849 (1998).

5. W.Y. Tam and G. Ahlers, *Phys. Rev. B* **32**, 5932 (1985); **33**, 193 (1986).

6. M. Dingus, F. Zhong, and H. Meyer, *J. Low Temp. Phys.* **65**, 185 (1986); M. Dingus, F. Zhong, J. Tuttle, and H. Meyer, *J. Low Temp. Phys.* **65**, 213 (1986).

7. For a review, see V. Dohm, *Z. Phys. B* **60**, 61 (1985).

8. R. Haussmann and V. Dohm, *Phys. Rev. Lett.* **67**, 3404 (1991); *Z. Phys. B* **87**, 229 (1992).

9. R. Haussmann and V. Dohm, *J. Low Temp. Phys.* **89**, 429 (1992); *Phys. Rev. B* **46**, 6361 (1992).

10. R. Haussmann, *J. Low Temp. Phys.* **114**, 1 (1999).

11. P. Weichman, A. Prasad, R. Mukhopadhyay, and J. Miller, *Phys. Rev. Lett.*, **80,** 22 (1997); P. Weichman and J. Miller, preprint..

12. T.C.P. Chui, D.L. Goodstein, A. W. Harter, and R. Mukhopadhyay, *Phys. Rev. Lett.*, **77,** 1793 (1996).

13. P. Day, W. Moeur, S. McCready, D. Sergatskov, and R. Duncan, *Phys. Rev. Lett.*, **81,** 2474 (1998).

14. W.A. Moeur, P.K. Day, F-C. Liu, S.T.P. Boyd, M.J. Adriaans, and R.V. Duncan, *Phys. Rev. Lett.*, **78,** 2421 (1997).

15. F-C. Liu and G. Ahlers, *Physica (Amsterdam)* **194B - 196B**, 597 (1994).

16. A. Onuki, *J. Low Temp. Phys.* **50**, 433 (1983).

17. A. Harter *et al.*, preprint.

18. For a collection of reviews on various aspects of critical phenomena, see C. Domb and M.S. Green, Phase transitions and Critical Phenomena (Academic Press, 1976) and references therein.

19. R.A. Ferrell, N. Menyhard, H. Schmidt, F. Schwabl, and P. Szepfalusy, *Phys. Rev. Lett.* **18**, 891 (1967); *Phys. Lett.* **24A**, 493 (1967); *Ann. Phys. (NY)* **47**, 565 (1968).

20. G. Ahlers, *Phys. Rev. Lett.* **21**, 1159 (1968).

21. J. Kerrisk and W.E. Keller, *Phys. Rev*. **117**, 341 (1969).

22. A. Singsaas and G. Ahlers, *Phys. Rev. B* **30**, 5103 (1984). In the nonlinear region we do not distinguish between the correlation length above and below the transition.

23. H.J. Mikeska, *Phys. Rev*. **179**, 166 (1969).

24. G.B. Hess, *Phys. Rev. Lett*. **40**, 1191 (1978).

25. B.I. Halprin, P.C. Hohenberg, and E.D. Siggia, *Phys. Rev. Lett*. **32**, 1289 (1974); *Phys. Rev. B* **13**, 1299 (1976).

26. V. Dohm and R. Folk, *Phys. Rev. Lett*. **46,** 349 (1981).

27. G. Ahlers, *Phys. Rev*. **171**, 275 (1968).

28. F-C. Liu, R.V. Duncan, U. Israelsson, T. Chui, D. Hensinger, A. Nash, M. Adriaans, and W. Moeur, *Czech. J. Phys. Suppl. S1* **46**, 87 (1996).

29. R.V. Duncan, G. Ahlers, and V. Steinberg, *Phys. Rev. Lett*. **60**, 1522 (1988).

30. H. Baddar, G. Ahlers, K. Kuehn, and H. Fu, preprint.

31. C.J. Gorter and J.H. Mellink, *Physica* **15**, 285 (1949).

32. B.J. Klemme, M.J. Adriaans, P.K. Day, D.A. Sergatskov, T.L. Aselage, and R.V. Duncan, *J. Low Temp. Phys*. **116**, 133 (1999).

33. F-C. Liu and G. Ahlers, *Phys. Rev. Lett*. **76**, 1300 (1996).

34. D. Murphy and H. Meyer, *Phys. Rev. B* **57**, 536 (1998).

35. See, for example, J. Wilks, The Properties of Liquid and Solid Helium (Oxford Press, 1967).

36. W.A. Moeur, P.K. Day, F-C. Liu, S.T.P. Boyd, M.J. Adriaans, and R.V. Duncan, unpublished.

37. R.V. Duncan, P.K. Day, S.S. McCready, W.A. Moeur, F-C. Liu, and D.A. Sergatskov, *J. Low Temp. Phys*. **113**, 861 (1998).

38. R.V. Duncan, P.K. Day, D. Elliott, D.A. Sergatskov, and A. Babkin, *Physica* to appear (2000).

39. S.S. McCready and S.T.P. Boyd, DYNAMX Design File DX-DF-120, unpublished.

40. S.T.P. Boyd, unpublished.

41. R. V. Duncan, D.A. Sergatskov, S.T.P. Boyd, S.S. McCready, T.D. McCarson, A.V. Babkin, P.K. Day, F-C. Liu, and D. Elliott, to appear in *J. Low Temp. Phys*.

42. Vespel is a registered trademark of the DuPont Corporation.

43. P. Day, I. Hahn, and T.C.P. Chui, *J. Low Temp. Phys.* **107**, 359 (1997).

44. R.V. Duncan, G. Ahlers, and V. Steinberg, *Phys. Rev. Lett*. **58**, 377 (1987).

45. Quang Li, Ph.D. Thesis, Stanford University, 1990; Q. Li and J.A. Lipa, unpublished.

46. Andrew Chatto, within Prof. David Goodstein's Group at Caltech (unpublished).

## 9.0      List of Acronyms and Symbols

| | |
|---|---|
| **ATP** | Authority to Proceed |
| **CDR** | Critical Design Review |
| **CHeX** | Confined Helium Experiment (PI: Lipa) |
| **CP** | Charged Particle |
| **CPM** | Charged Particle Monitor |
| **DX-DF-xxx** | DYNAMX Design File entry numer xxx (available from UNM or JPL on request) |
| **DYNAMX** | Critical Dynamics in Microgravity |
| **EMI** | ElectroMagnetic Interference |
| **FP** | Fundamental Physics |
| **FRD** | Functional Requirements Document |
| **GRT** | Germanium Resistance Thermometer |
| **GSE** | Ground Support Equipment |
| **He-I** | Normal Fluid Phase of $^4$He |
| **He-II** | Superfluid Phase of $^4$He |
| **HRT** | High Resolution Thermometer |
| **IGV** | Instrument Guard Vacuum |
| **ISP** | Integrated Sensor Package |
| **ISS** | International Space Station |
| **JPL** | Jet Propulsion Laboratory |
| **JSC** | Johnson Space Center |
| **KSC** | Kennedy Space Center |
| **LOA** | List of Acronyms |
| **LPE** | Lambda Point Experiment (PI: Lipa) |
| **LTMPF** | Low Temperature Microgravity Physics Facility |
| **M1** | First LTMPF Mission, M2 is the second mission, etc. |
| **MiniHRT** | Miniature High-Resolution Thermometer |
| **MRPO** | Microgravity Research Program Office (MSFC) |
| **MSFC** | Marshall Space Flight Center |
| **NASA** | National Aeronautic and Space Administration |
| **NASDA** | National Space Development Agency of Japan |
| **NRA** | NASA Research Announcement |
| **PI** | Principal Investigator |
| **Q** | Heat Flux |
| **ΔQ** | Additional Heat Flux Applied to Advance the Interface |
| **RDR** | Requirements Definition Review |
| **SAA** | South Atlantic Anomaly |
| **SCR** | Science Concept Review |
| **SAMS** | Space Acceleration Measurement System |
| **SQUID** | Superconducting Quantum Interference Device |
| **SRD** | Science Requirements Document |
| **SRED** | Science Requirements Envelope Document |
| **t** | Reduced Temperature |

| | |
|---|---|
| $\tau$ | Time |
| **T** | Temperature |
| $T_c(Q)$ | Temperature where Superfluid Counterflow Heat Transport Catastrophically Fails |
| $T_\lambda$ | Static Superfluid Transition Temperature |